Spatial organization of heterogeneous immunotherapy target antigen expression in high-grade glioma

Michael E. Barish [a,#,*]; Lihong Weng [b,#]; Dina Awabdeh [a]; Yubo Zhai [b]; Renate Starr [b]; Massimo D'Apuzzo [c]; Russell C. Rockne [d]; Haiqing Li [e]; Behnam Badie [f]; Stephen J. Forman [b]; Christine E. Brown [b,g,*]

[a] Department of Stem Cell Biology & Regenerative Medicine, Beckman Research Institute, City of Hope, Duarte, CA 91010, United States
[b] Department of Hematology & Hematopoietic Cell Transplantation, National Medical Center, City of Hope, Duarte, CA 91010, United States
[c] Department of Pathology, National Medical Center, City of Hope, Duarte, CA 91010, United States
[d] Department of Computational and Quantitative Medicine, Division of Mathematical Oncology, Beckman Research Institute, City of Hope, Duarte, CA 91010, United States
[e] Integrative Genomics Core, Division of Translational Bioinformatics, Beckman Research Institute, City of Hope, Duarte, CA 91010, United States
[f] Department of Surgery, Division of Neurosurgery, National Medical Center, City of Hope, Duarte, CA 91010, United States
[g] Department of Immuno-Oncology, Beckman Research Institute, City of Hope, Duarte, CA 91010, United States

Abstract

High-grade (WHO grades III-IV) glioma remains one of the most lethal human cancers. Adoptive transfer of tumor-targeting chimeric antigen receptor (CAR)-redirected T cells for high-grade glioma has revealed promising indications of anti-tumor activity, but objective clinical responses remain elusive for most patients. A significant challenge to effective immunotherapy is the highly heterogeneous structure of these tumors, including large variations in the magnitudes and distributions of target antigen expression, observed both within individual tumors and between patients. To obtain a more detailed understanding of immunotherapy target antigens within patient tumors, we immunochemically mapped at single cell resolution three clinically-relevant targets, IL13Rα2, HER2 and EGFR, on tumor samples drawn from a 43-patient cohort. We observed that within individual tumor samples, expression of these antigens was neither random nor uniform, but rather that they mapped into local neighborhoods – phenotypically similar cells within regions of cellular tumor – reflecting not well understood properties of tumor cells and their milieu. Notably, tumor cell neighborhoods of high antigen expression were not arranged independently within regions. For example, in cellular tumor regions, neighborhoods of high IL13Rα2 and HER2 expression appeared to be reciprocal to those of EGFR, while in areas of pseudopalisading necrosis, expression of IL13Rα2 and HER2, but not EGFR, appeared to reflect the radial organization of tumor cells around hypoxic cores. Other structural features affecting expression of immunotherapy target antigens remain to be elucidated. This structured but heterogeneous organization of antigen expression in high grade glioma is highly permissive for antigen escape, and combinatorial antigen targeting is a commonly suggested potential mitigating strategy. Deeper understanding of antigen expression within and between patient tumors will enhance optimization of combination immunotherapies, the most immediate clinical application of the observations presented here being the importance of including (wild-type) EGFR as a target antigen.

* Corresponding authors.
E-mail addresses: mbarish@coh.org (M.E. Barish), cbrown@coh.org (C.E. Brown).
\# Shared first authorship

Introduction

The present standard of care for high-grade glioma (WHO grades III-IV) remains maximal surgical resection followed by a combination of radiation, chemotherapy [1], and electric field stimulation [2]. Unfortunately, despite considerable efforts, achieving effective and durable responses to treatment has remained elusive [3].

Immunotherapies in various forms [4], among them chimeric antigen receptor (CAR) T cell immunotherapy [5–12], have provided tantalizing evidence of clinical responses [9,13] that, almost inevitably, have been followed by tumor recurrence. Failure to achieve satisfactory clinical responses has been attributed to multiple tumor responses initiated by the selection pressures imposed by immunotherapies, including, but not limited to, enhancement of the already highly disseminated nature of high grade glioma, activation of resistance mechanisms originating in the tumor microenvironment [9,14], and the potential for evasion of immune targeting (antigen escape) conferred by phenotypic heterogeneity within tumors [15–20].

Work over the last several decades has revealed complex spatially heterogeneous distributions of genetic, epigenetic, metabolic and protein expression patterns that collectively define local neighborhoods within brain tumors [21]. We believe that fine-grained cell-level analyses across multiple patients will be required to achieve the level of understanding of high-grade glioma [22] required to design the most effective therapies.

Immunotherapies ideally target tumor-associated antigens with elevated expression on glioma cells with little or no confounding expression on normal cells in the brain or elsewhere. Several antigens fulfilling this requirement have been described, proposed, or are under evaluation, in ongoing clinical trials of chimeric antigen receptor (CAR) redirected T cells: IL13Rα2 [16,23]; HER2 [24–26]; EphA2 [27]; and wild-type EGFR as well as the EGFRvIII variant [28–30].

Our laboratories have focused on acquiring a deeper understanding of the organization of cell populations within the tumors of individual patients (intra-tumor heterogeneity), and of how these vary between different patients (inter-patient variability). In this study we consider spatial expression three immunotherapy target antigens across a cohort of patient samples: IL13Rα2, HER2 and EGFR. IL13Rα2 is a high-affinity IL13 receptor expressed by a high percentage of high-grade gliomas [23,31-34], but not significantly in normal brain. The HER2/ErbB2 receptor tyrosine kinase is expressed by 15-30% of GBMs and is not found on normal postnatal neurons and glial cells [35,36]. EGFR is over-expressed in well over half (55-70%) of newly diagnosed glioblastomas [37], with appearance of the EGFRvIII mutation, when present, overlapping with wild-type EGFR [38–40]. Immunological targeting of IL13Rα2, HER2 and EGFR individually has been shown to be safe in clinical practice [16,26,28].

We have here defined by immunochemistry the spatially-varying expression patterns of these three immunotherapy targets in formalin-fixed paraffin-embedded (FFPE) tissue samples from a cohort of 43 patients with high-grade glioma (WHO grades III-IV). We observed that when examined at cell-level resolution, target antigen expression was for the most part organized into millimeter-scale neighborhoods – phenotypically similar cells within regions of cellular tumor [21] –shaped by not well understood combinations of cell intrinsic processes and impinging microenvironmental cues. Strikingly, when considered across cellular tumor areas of many patient samples, the spatial extent of EGFR-dominant neighborhoods appeared be reciprocal to the distribution of IL13Rα2 and HER2. Areas of pseudopalisading tumor cells, however, showed tighter spatial organization in which expression of IL13Rα2 and HER2 could vary over a few cell diameters in cells arrayed around hypoxic centers [41]. Curiously, in these areas of pseudopalisading tumor cells, EGFR expression appeared independent of the hypoxic gradients presumed to shape IL13Rα2 and HER2 expression.

In future investigations of fundamental tumor biology we will consider the multiple overlapping mechanisms that together shape the organization of these antigen expression neighborhoods. Clinically, our data suggests that optimal multiantigen targeting strategies to "box in" high-grade gliomas and minimize antigen escape to yield more effective and durable therapeutic responses [42–44] should incorporate targeting of (wild-type) EGFR.

## Materials and methods

Patient samples

A cohort of 43 deidentified high-grade glioma brain tumor samples (Supplemental Table 1), unselected except for the size of the tissue section, were drawn from archival material in the tumor bank maintained by the COH Department of Pathology: 25.6% (11/43) WHO grade III and 74.4% (32/43) WHO grade IV. Brain tumor samples were acquired at resection or biopsy from patients with either progressing or recurrent tumors (the patient populations available to us), and therefore from patients previously exposed to other therapies but who had not initiated immunotherapy. At the time that most of these tumor samples were collected, between 2004 and 2013, information on IDH status, EGFR amplification, TCGA subtype, and other tumor characteristics was not collected and therefore, while potentially informative, was not available. Some information on the tumors was incorporated in pathology reports, and is presented in Supplementary Table 1. As controls, five normal human brain samples were purchased from US Biomax (GL803), and four normal brain tissue samples (frontal cortex, hippocampus, medulla, and pons) were provided by the City of Hope Department of Pathology. All procedures and protocols were approved by the City of Hope Institutional Review Board (IRB).

Immunohistochemical staining

Serial 4 μm-thick sections were cut from formalin-fixed, paraffin-embedded (FFPE) blocks to generate sequential slides for multiple antigen staining. In each case, the first slide was processed for hematoxylin and eosin (H&E) staining, followed by (in sequence) EGFR, IL13Rα2, and HER2 immunohistochemistry (IHC), each with hematoxylin counterstain, using Envision+System-HRP 3,3′-diaminobenzidine (DAB) chemistry and AutostainerPlus hardware (both Dako) by the City of Hope Research Pathology Core shared resource. All patient sample and control slides were processed together to minimize batch effects. Antibodies and dilutions were: EGFR (1:100, Invitrogen 28-0005); IL13Rα2 (1:600, R&D Systems AF146); HER2 (1:200, Dako A0485). Cell populations identified by EGFR immunoreactivity likely included those displaying the EGFRvIII variant, as EGFRvIII expression is almost always associated with wild-type EGFR [38–40].

Visual evaluation of tumor grade and antigen expression

For each of the 43 patient tumor samples, the H&E slide was annotated by a neuropathologist (D'Apuzzo) to define four major histological regions: cellular tumor (defined as >60% tumor cells), pseudopalisading within cellular tumor areas, infiltrating tumor (<50% tumor cells), and normal brain (approximately 0% tumor cells). Intensity scales for each antigen were set based on positive and negative controls: testis and prostate tissue for IL13Rα2, and breast cancer and lung cancer for HER2 and EGFR, respectively. Visual scoring of antigen expression (H score = 0-300) used the system: intensity (1-3) × percent positive cells.
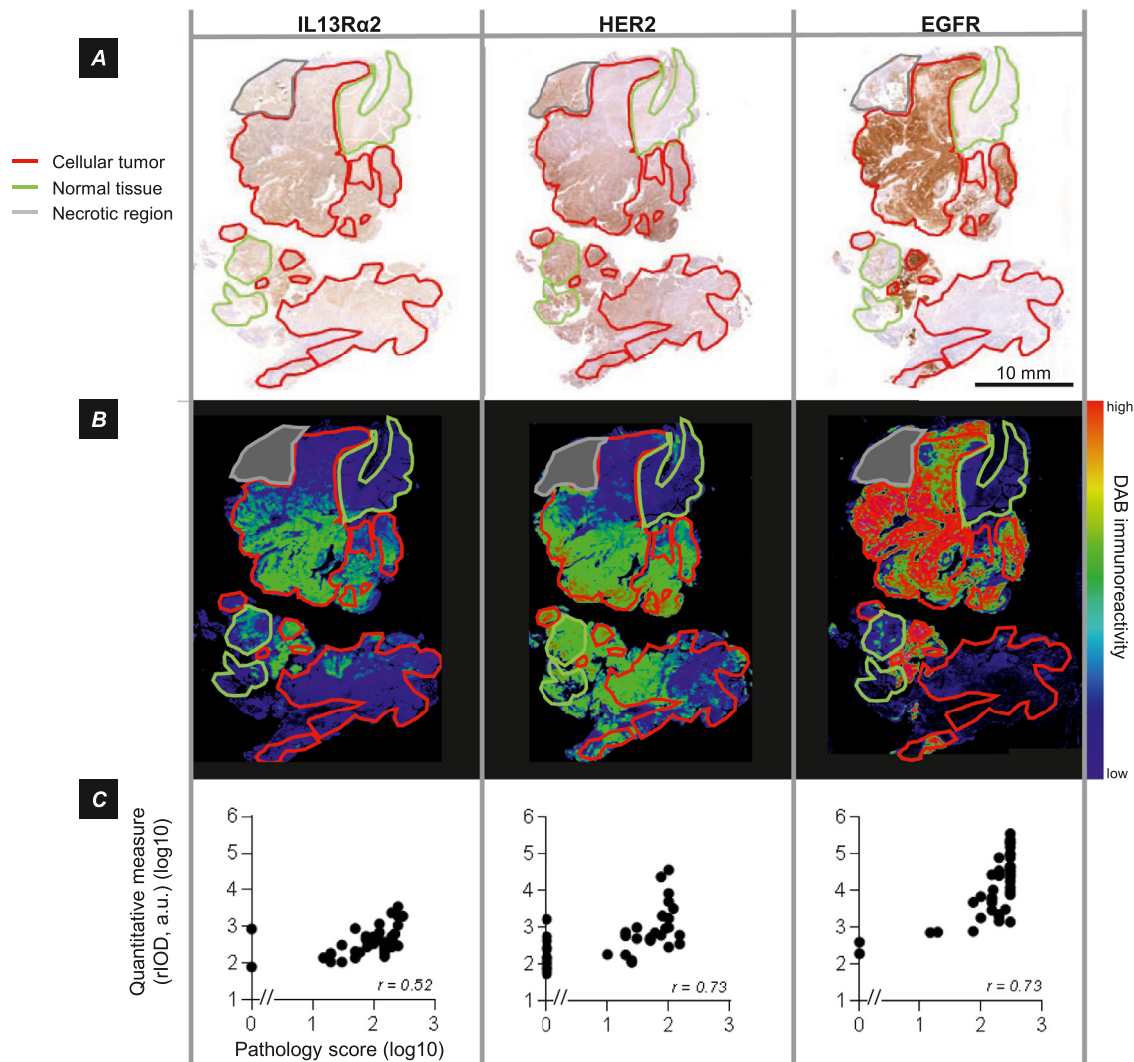
Figure 1. Spatially varying expression of immunotherapy target antigens IL13Rα2, HER2 and EGFR. **A,** Immunohistochemical (DAB) visualization of target antigens in aligned serial sections, annotated for cellular tumor regions as well as for normal and necrotic regions, illustrating variation in their expression across the tumor section. Note in these sections the absence of immunostaining for CAR T cell target antigens in regions of normal brain. Tumor PBT025-1 **B,** DAB optical density for images in part A, pseudocolored blue (low) → red (high). The same color scale was used for each image. **C,** Overall agreement of visual immunostaining score by a neuropathologist [H score = intensity (1-3) × percent positive cells], and quantitative measures of regional integrated optical density (rIOD) for the same tumor sections. Spearman coefficients are indicated; $p = <0.001$ for all comparisons.

High resolution slide scanning

The stained tumor sections were imaged in their entirety at high resolution (0.46 × 0.46 μm pixels) using a Hamamatsu Nanozoomer 2.0 HT scanner (20 × source lens) (City of Hope Light Microscopy and Digital Imaging Core). Images were saved in NDPI format (Hamamatsu) and examined with NDPI.view v2 (Hamamatsu) or ImagePro Premier v9.1 (Media Cybernetics). For quantitative measurements, images were downsampled 1:4 (to 1.84 × 1.84 μm pixels) and converted to TIFF format (Icy; http://icy.bioimageanalysis.org/), and then deconvolved into DAB and hematoxylin (nuclear counter stain) channels (Fiji/ImageJ; https://fiji.sc/) [45].

*Quantitative considerations of target antigen expression*

Images of serial sections were brought into registration using a two-step process. First, the images of deconvolved hematoxylin-stained nuclei were optimized for contrast and aligned [Fiji/ImageJ; Register Virtual Stack Slices

(affine feature extraction, elastic registration by bUnwarpJ splines)]. Then the transformation parameters for the nuclear images were applied to the immunostained (DAB) sections (Fiji/ImageJ; Transform Virtual Stack Slices). The segmented immunostained images could then be pseudocolored and superimposed.

To examine histological regions of interest (ROIs) identified from H&E stained slides (cellular tumor, for example), ROIs were mapped onto sequential immunostained sections for region-specific analyses. Expression levels of EGFR, IL13Rα2 and HER2 in these ROIs were measured as regional integrated optical density (rIOD) using the DAB plug-in of ImagePro. Within each histologically-defined ROI, ImagePro identified features as areas of grouped immunostained pixels, and for each feature returned integrated optical density (IOD) and feature area. Values of rIOD, IOD scaled to the feature area within each ROI, were calculated as 255 − [(ΣIOD / Σarea) × (average area)]. These values of rIOD were used as metrics of antigen expression within histologically-defined regions. The threshold for positive expression of each antigen was two times the average rIOD determined for a cohort of normal brain controls (Figure 6B).
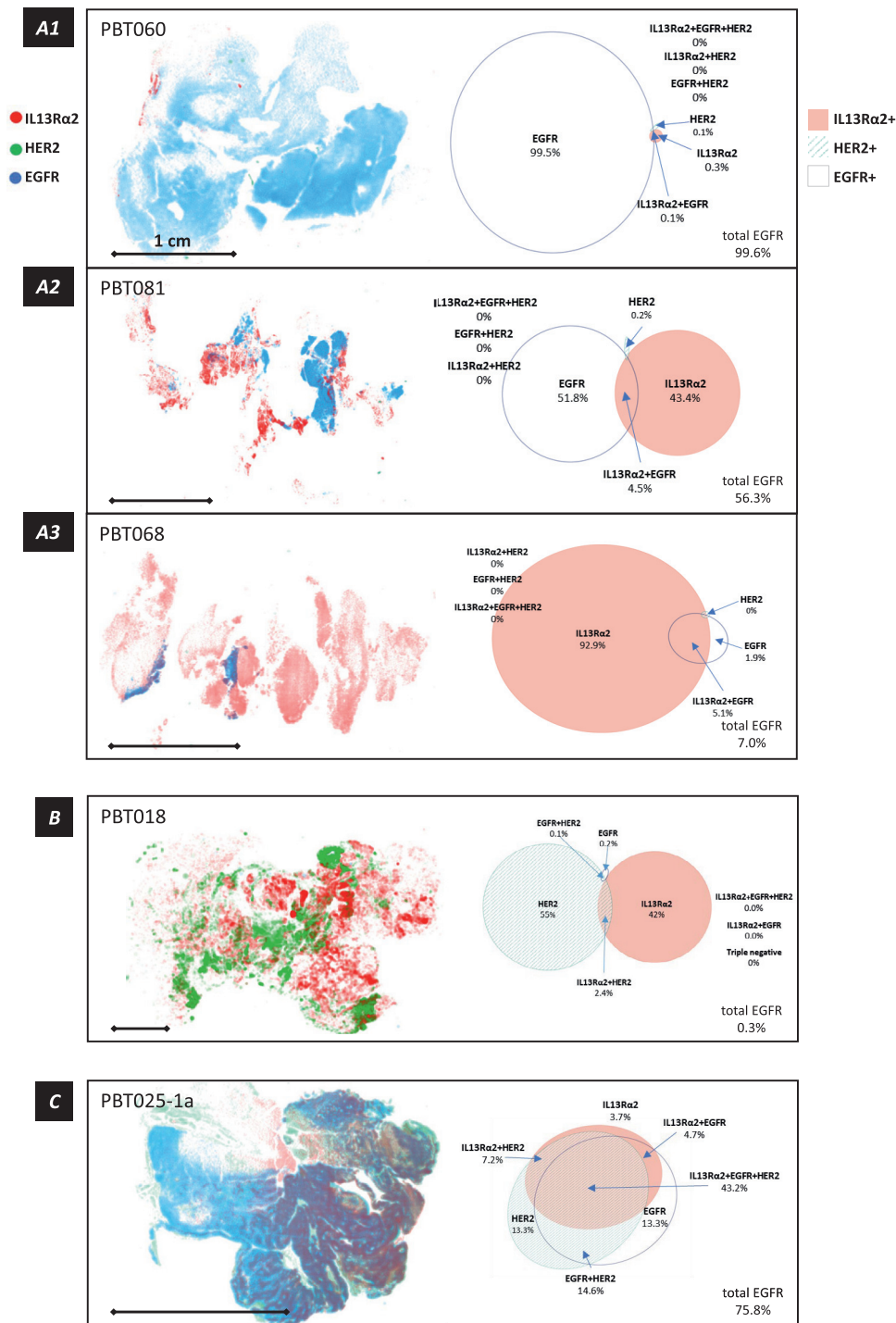
Figure 2. Intra-tumoral organization of IL13Rα2, HER2 and EGFR antigen expression neighborhoods in cellular tumor regions, as determined from a grid superimposed on aligned serial sections. Within each grid element (9.2 × 9.2 µm), optical density (OD) for IL13Rα2 (red), HER2 (green) and EGFR (blue) was measured, scaled relative to the maximum value in that section, and plotted with OD determining symbol size [smaller (lower) → larger (higher)], and transparency [more transparent (lower) → more opaque (higher)]. For clarity of these plots, the threshold for display was 30% of maximum, and grid elements were binned 10:1. Associated with each map is an Euler diagram presenting the proportions of cellular tumor regions in each tumor section occupied by each of the eight possible antigen combinations. Scale bar = 1 cm in each panel. **A1-A3,** Three tumor samples (with relatively low HER2 expression) illustrating tumor-to-tumor progression from EGFR-dominant to IL13Rα2-dominant antigen expression. **B,** A tumor sample (PBT018) with very low EGFR expression, illustrating intermixing with relatively little high level co-expression in IL13Rα2- and HER2-dominant neighborhoods. **C,** A portion of tumor sample PBT025-1 with extensive pseudopalisading necrosis (PBT025-1a), showing the relation between the structure of the tumor cell palisades and target antigen expression (considered in more detail in Figure 4). The Euler diagram illustrates the extensive overlap of antigen expression within this subregion of pseudopalisading necrosis.
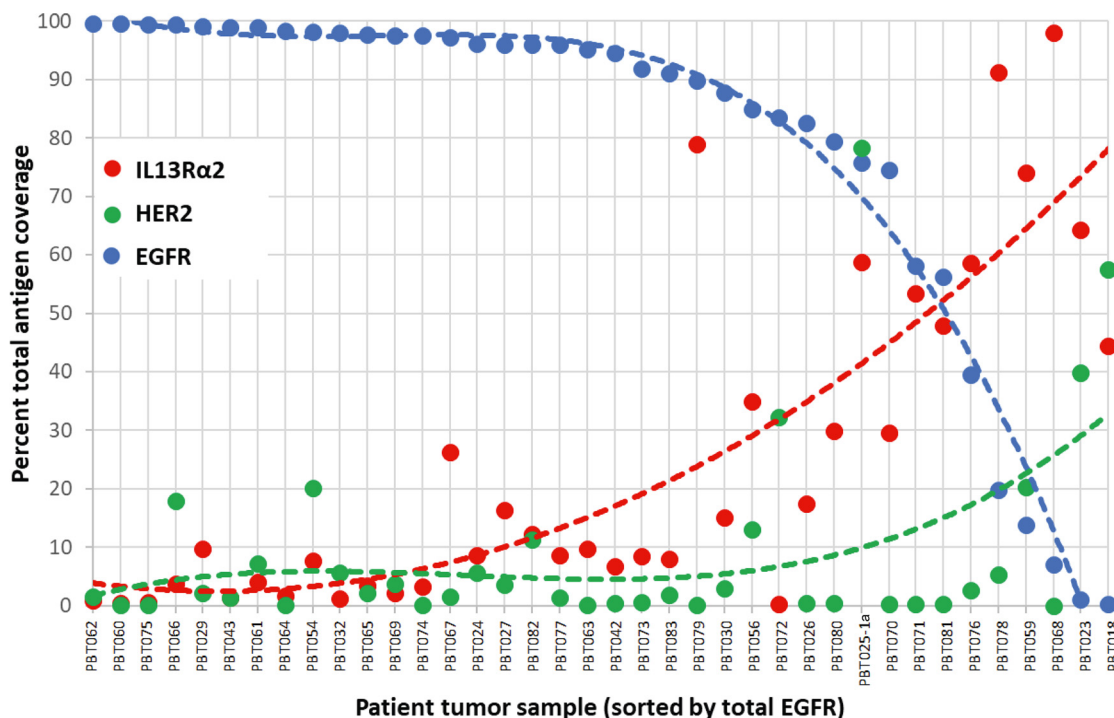
Figure 3. Total percent of cellular tumor regions in each section occupied by each of the targeted antigens (IL13Rα2, HER2 and EGFR), ordered by total EGFR occupancy. Data are shown for the entirety of tumor samples, with the exception of PBT025a encompassing the area of pseudopalisading necrosis, and illustrate the overall reciprocal relationship between expression of EGFR and IL13Rα2 (and to some extent HER2). The complete set of antigen immunoreactivity maps from which these values were taken are shown in Supplemental Figure 1. The dotted lines highlight trends in the data.

Alternatively, to evaluate IL13Rα2, HER2 and EGFR expression in regions of each tumor without prior selection of ROIs, a grid (5 × 5 pixels; 9.2 × 9.2 μm; total area 84.64 μm²) was imposed on the IL13Rα2/HER2/EGFR TIFF image stack, and OD was extracted for each antigen in each position. These were then plotted (down-sampled 10:1 for efficiency) using Origin (Origin Lab; Northampton, MA) with the presence of each antigen in each position indicated by color, and staining intensity (OD) by symbol size and transparency (Figure 2; Supplementary Figure 1) . Proportions of total cellular tumor area occupied by each of the eight possible combinations of three tumor antigens were computed for each position in the grid, and visualized in Euler diagrams (Euler*APE*) [46] (Figures 2 and 6C; Supplementary Figure 1). Additionally, we determined the total percent of tumor area occupied by each antigen, singly or in combination (Figure 3).

Statistical considerations

Statistical significance was evaluated in Prism v8 (GraphPad Software) by Student's *t*-test; significance was assessed as $p < 0.05$.

The Spearman correlation coefficient (r) for non-parametric data, calculated using Prism v8, was used to compare software-based quantification with conventional pathology scores (Figure 1C), to compare expression levels of IL13Rα2, HER2 and EGFR between tumor samples (Figure 7A), and to evaluate The Cancer Genome Atlas (TCGA) [47] expression data (Figure 7B). TCGA mRNA expression levels (Affymetrix U133A array) were determined using probes 206172_at for IL13Rα2, 216836_s_at for ERBB2, and 201983_s_at for EGFR, with threshold defined as 2-fold over-expression compared to normal brain.

The Shannon diversity index (*H*) is a metric, viewed in an ecological context, of species diversity within a mixed population of many species. It incorporates consideration of the number of species in the population (richness) and their relative abundance (evenness). Here, for cellular tumor regions, *N* is the number of antigen species, in this case three (IL13Rα2, HER2, and EGFR), and p_i (calculated from relative rIOD) is the proportional expression of each antigen within a given region or neighborhood. It is evaluated as $H = \sum_{i=1}^{N} p_i \ln(p_i)$. Thus an *H* value of 0 indicates no diversity (one antigen present), and increasing values of *H* reflect the presence of both multiple antigens and greater differences in their relative expression.

Results

Expression of potential immunotherapy target antigens was evaluated in individual surgical resections from a 43-patient cohort (Supplemental Table 1). For each tumor sample, consecutive FFPE sections were H&E stained, or immunostained for the immunotherapy target antigens of interest: IL13Rα2, HER2, and EGFR. From the H&E sections, a neuropathologist outlined histologically-defined regions of normal brain, infiltrating tumor, cellular tumor, pseudopalisading necrosis (a subset of cellular tumor), and necrotic tissue that was omitted from any further analyses. In the example of immunostained sections shown in Figure 1A (PBT025-1) and presented in pseudocolor in Figure 1B, it is clear that within cellular tumor regions, expression of IL13Rα2, HER2 and EGFR could be intermixed and not spatially uniform.

In this study we evaluated antigen expression by pixel-level quantitative measures of DAB-visualized immunoreactivity, expressed as regional integrated optical density (rIOD) in tumor regions, or as OD within elements of grids superimposed on regions of cellular tumor. The comparisons presented in Figure 1C confirm that rIOD measurements and visual scoring (H scoring) show similar trends and significant correlation ($p = <0.001$ for each of the three antigens). Note that quantitative measures of antigen expression revealed fine distinctions within the cellular tumor regions visually assigned a score of zero.
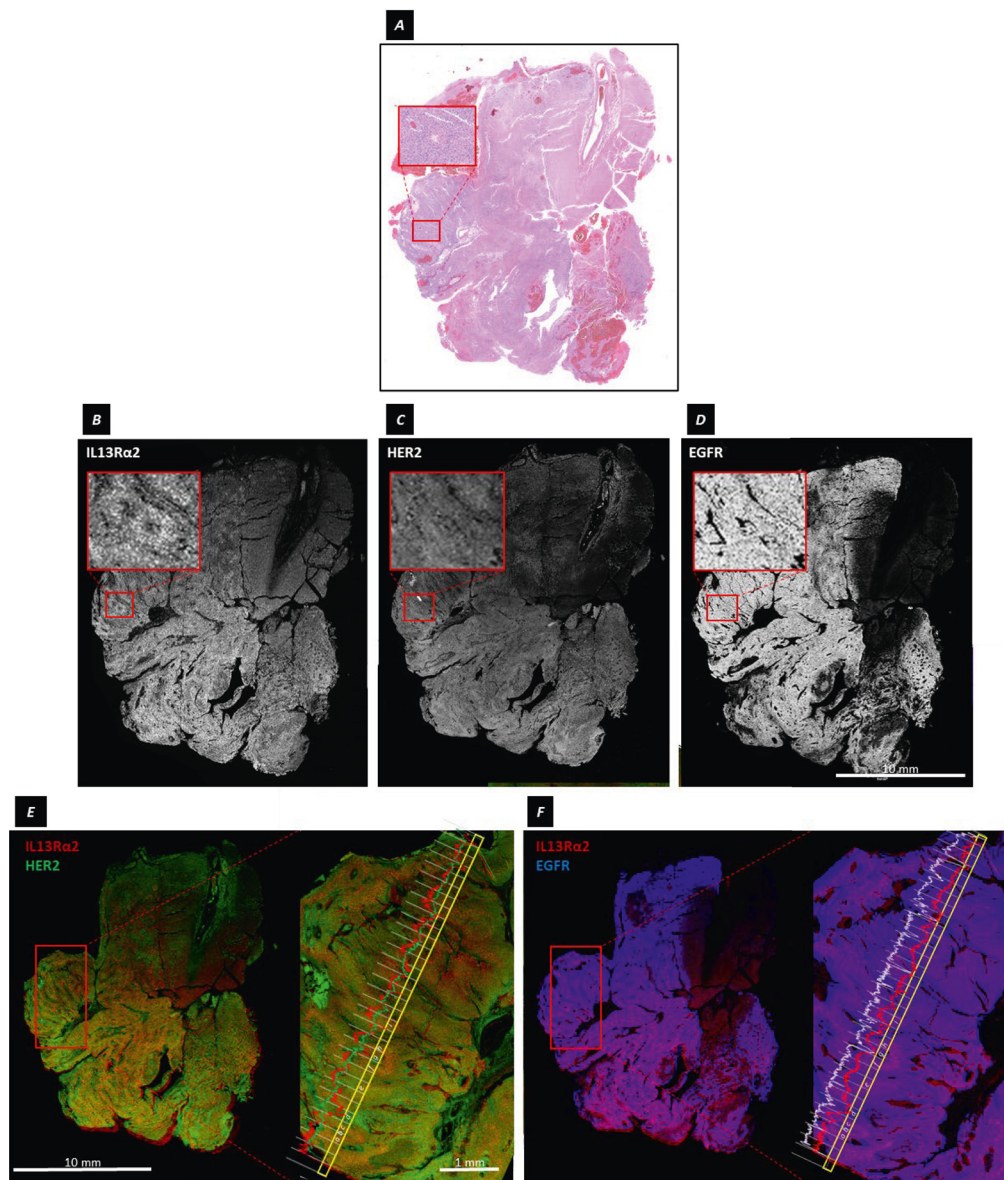
Figure 4. Differing microgranularity of IL13Rα2, HER2 and EGFR expression at the resolution of single pixels. **A**, H&E stained section of tumor sample PBT025-1a. The inset shows a subregion of pseudopalisading necrosis within the region of cellular tumor. **B-D**, Gray-scale images of aligned serial sections immunostained for IL13Rα2,HER2, and EGFR. The insets show the subregion of pseudopalisading necrosis, and illustrate in **B** rapid variation of IL13Rα2 immunoreactivity over a few cell diameters around the presumably hypoxic core, (**C**) more dispersed HER2 immunoreactivity, and (**D**) relatively uniform EGFR immunoreactivity. **E-F**, Superimposed aligned tumor sections showing (**E**) IL13Rα2 and HER2, and (**F**) IL13Rα2 and EGFR. The enlarged images on the right of **E** and **F** are the subregion of pseudopalisading necrosis, with a transect (yellow) and plot of OD across each pixel-length portion of the transect averaged across its width. Along the transect in **E**, the ODs of IL13Rα2 (red) and HER2 (green) immunostaining varied with the architecture of the pseudopalisades, although not necessarily in parallel (compare *c* at the peak of the palisade with *d* in the trough, or *g* and *h*). Along the same transect in **F**, the OD of EGFR (blue-white) immunostaining remained essentially constant except when the transect crossed areas of low cellularity (*d, g*).
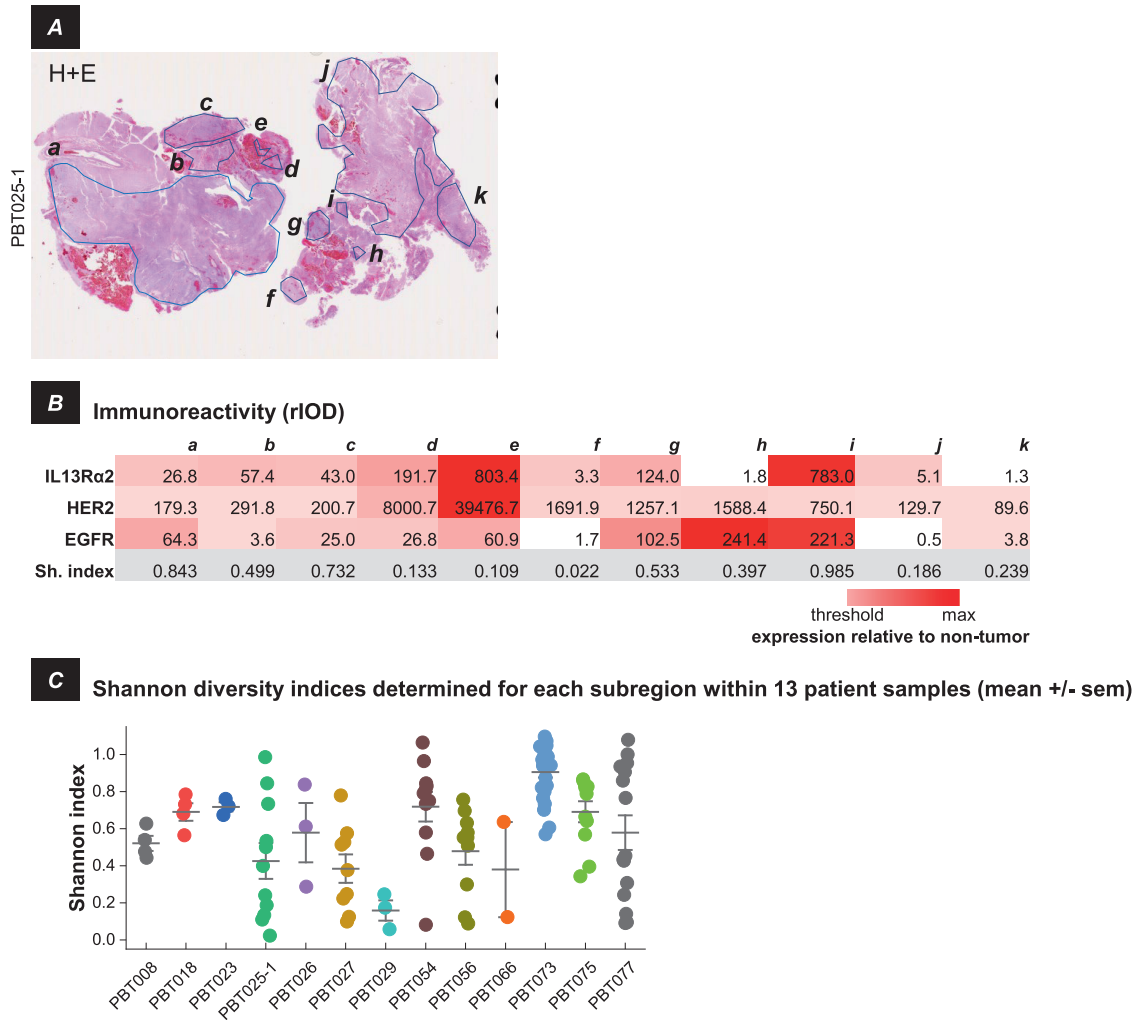
Intra-tumoral heterogeneity

We examined variations in antigen expression within cellular tumor regions of patient samples using three approaches: an arbitrarily imposed grid, a structural morphology highly characteristic of glioblastoma (WHO grade IV), and subregions identified by image analysis software.

(a) Antigen expression within elements of an imposed grid

We mapped antigen expression across cellular tumor regions by arbitrarily superimposing a grid onto the aligned sections of each of the 38 patient tumors for which this analysis was possible, with each element a 5×5 square of 1.84×1.84 μm pixels (9.2×9.2 μm; total area of 84.6 μm^2). The optical density (OD) for each antigen averaged across each grid element was then determined and mapped. Five illustrative examples of alternative expression patterns are presented in Figure 2; the entire series of patient samples is presented in Supplemental Figure 1. In these maps, for visual clarity grid elements were binned 10:1 (92×92 μm; 8,464 μm^2), and average OD in each binned element is represented in diameter and opacity. For each antigen, the threshold for display was 30% of maximum OD, emphasizing neighborhoods of higher antigen expression. Adjacent Euler diagrams plot

Figure 5. Intra-tumoral heterogeneity of IL13Rα2, HER2 and EGFR antigen expression within separate subregions of cellular tumor. **A,** H&E section of tumor sample PBT025-1, with 11 separate cellular tumor subregions identified by the DAB plug-in of ImagePro, outlined and labeled *a-k*. **B,** Immunoreactivity (rIOD) within each of these subregions, colored in the table white (below threshold) → red (maximum). The bottom row shows the Shannon diversity index (Sh. Index) calculated for each of the subregions, with higher numbers indicating greater diversity. **C,** Shannon diversity indices for separate subregions within cellular tumor regions of each of 13 patient samples for which these could be identified. Data are mean +/- s.e.m.

the percentages of the total cellular tumor area occupied by each of the eight combinations of the three antigens.
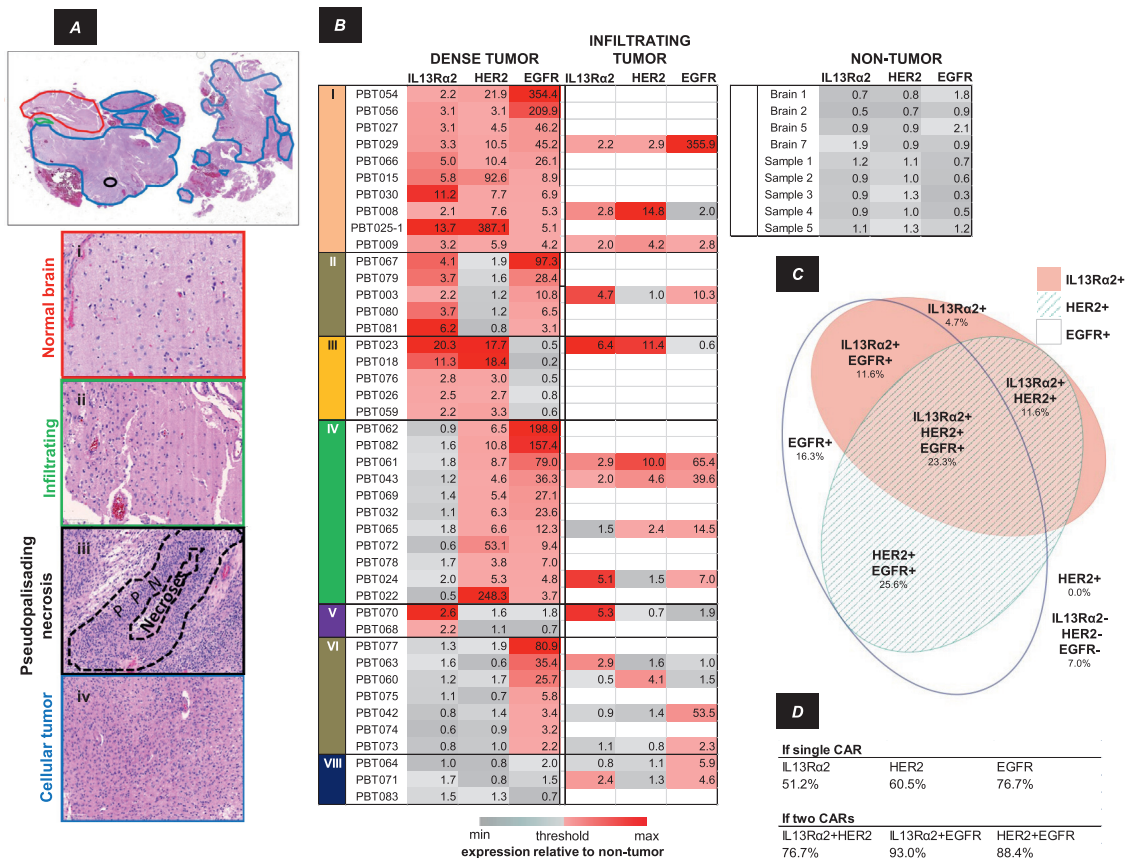
These expression maps demonstrate non-random and non-independent antigen expression in neighborhoods within cellular tumor regions, with for the most part little spatial overlap in areas with the highest antigen expression levels. In one common pattern, illustrated in Figure 2A1-A3, there is a progression from high EGFR to high IL13Rα2 spatial occupancy, with relatively few neighborhoods of high HER2 expression. In the cellular tumor regions with the lowest EGFR occupancy, PBT018 (Figure 2B, Supplemental Figure 1) and PBT023 (Supplemental Figure 1), neighborhoods of high HER2 and IL13Rα2 immunostaining were intermixed; this is a pattern never seen when EGFR immunostaining was prominent except in a single case, PBT079 (Supplemental Figure 1). Pseudopalisading necrosis (Figure 2C), however, imposed a different antigen expression pattern that closely followed tumor morphology (considered in more detail below).

When examined across all 38 tumor samples, a progression from high to low percentage of total EGFR occupancy (determined from the Euler diagrams for each tumor) was accompanied by an inverse and reciprocal progression for IL13Rα2. This can be seen in Supplemental Figure 1, where

expression maps and Euler diagrams for cellular regions of the 38 tumor samples are ordered according to the total percentage area occupied by EGFR in each sample (high → low). Figure 3 presents these data graphically: in most cellular tumor regions, lower percentages of EGFR occupancy are associated with higher percentage coverage by IL13Rα2, and, at the lowest EGFR occupancies, HER2.

(b) Granularity of target antigen expression in an area of pseudopalisading necrosis

As noted above, the cellular tumor subregion of pseudopalisading necrosis (a cell architecture characteristic of GBM) in PBT025-1a (Figure 4A) presented a pattern in which IL13Rα2 and HER2 expression varied according to tumor architecture (evident in Figure 2C), and were organized around the central area of presumed hypoxia [41]. Within this space, IL13Rα2 immuoreactivity closely followed the radially-arranged contours of tightly packed tumor palisades (Figure 4B), with the distribution of HER2 immunoreactivity being somewhat more diffuse (Figure 4C) but still reflecting the underlying pseudopalisading structure. In contrast, EGFR immunoreactivity was more uniformly distributed (Figure 4D). As

Figure 6, Panel B — Target antigen rIOD relative to non-tumor tissues.

Group	Sample	Dense Tumor IL13Rα2	Dense Tumor HER2	Dense Tumor EGFR	Infiltrating Tumor IL13Rα2	Infiltrating Tumor HER2	Infiltrating Tumor EGFR
I	PBT054	2.2	21.9	354.4			
	PBT056	3.1	3.1	209.9			
	PBT027	3.1	4.5	46.2			
	PBT029	3.3	10.5	45.2	2.2	2.9	355.9
	PBT066	5.0	10.4	26.1			
	PBT015	5.8	92.6	8.9			
	PBT030	11.2	7.7	6.9			
	PBT008	2.1	7.6	5.3	2.8	14.8	2.0
	PBT025-1	13.7	387.1	5.1			
	PBT009	3.2	5.9	4.2	2.0	4.2	2.8
II	PBT067	4.1	1.9	97.3			
	PBT079	3.7	1.6	28.4			
	PBT003	2.2	1.2	10.8	4.7	1.0	10.3
	PBT080	3.7	1.2	6.5			
	PBT081	6.2	0.8	3.1			
III	PBT023	20.3	17.7	0.5	6.4	11.4	0.6
	PBT018	11.3	18.4	0.2			
	PBT076	2.8	3.0	0.5			
	PBT026	2.5	2.7	0.8			
	PBT059	2.2	3.3	0.6			
IV	PBT062	0.9	6.5	198.9			
	PBT082	1.6	10.8	157.4			
	PBT061	1.8	8.7	79.0	2.9	10.0	65.4
	PBT043	1.2	4.6	36.3	2.0	4.6	39.6
	PBT069	1.4	5.4	27.1			
	PBT032	1.1	6.3	23.6			
	PBT065	1.8	6.6	12.3	1.5	2.4	14.5
	PBT072	0.6	53.1	9.4			
		1.7	3.8	7.0			
	PBT024	2.0	5.3	4.8	5.1	1.5	7.0
	PBT022	0.5	248.3	3.7			
V	PBT070	2.6	1.6	1.8	5.3	0.7	1.9
	PBT068	2.2	1.1	0.7			
VI	PBT077	1.3	1.9	80.9			
	PBT063	1.6	0.6	35.4	2.9	1.6	1.0
	PBT060	1.2	1.7	25.7	0.5	4.1	1.5
	PBT075	1.1	0.7	5.8			
	PBT042	0.8	1.4	3.4	0.9	1.4	53.5
	PBT074	0.6	0.9	3.2			
	PBT073	0.8	1.0	2.2	1.1	0.8	2.3
VIII	PBT064	1.0	0.8	2.0	0.8	1.1	5.9
	PBT071	1.7	0.8	1.5	2.4	1.3	4.6
	PBT083	1.5	1.3	0.7			

Non-tumor:

Sample	IL13Rα2	HER2	EGFR
Brain 1	0.7	0.8	1.8
Brain 2	0.5	0.7	0.9
Brain 5	0.9	0.9	2.1
Brain 7	1.9	0.9	0.9
Sample 1	1.2	1.1	0.7
Sample 2	0.9	1.0	0.6
Sample 3	0.9	1.3	0.3
Sample 4	0.9	1.0	0.5
Sample 5	1.1	1.3	1.2

min — threshold — max
expression relative to non-tumor

Panel C (Euler diagram): IL13Rα2+ (red), HER2+ (hatched), EGFR+ (open)

- IL13Rα2+ 4.7%
- IL13Rα2+ EGFR+ 11.6%
- IL13Rα2+ HER2+ 11.6%
- IL13Rα2+ HER2+ EGFR+ 23.3%
- EGFR+ 16.3%
- HER2+ EGFR+ 25.6%
- HER2+ 0.0%
- IL13Rα2- HER2- EGFR- 7.0%

Panel D:

If single CAR

IL13Rα2	HER2	EGFR
51.2%	60.5%	76.7%

If two CARs

IL13Rα2+HER2	IL13Rα2+EGFR	HER2+EGFR
76.7%	93.0%	88.4%

If three CARs

IL13Rα2+HER2+EGFR
93.0%

Figure 6. Inter-patient heterogeneity of IL13Rα2, HER2 and EGFR expression within a cohort of 43 patients. **A,** H&E section annotated for four tissue characteristics as illustrated in the panels below: Normal brain (red), Infiltrating (green), Cellular (dense) tumor (blue), Pseudopalisading necrosis (black). **B,** Target antigen rIOD judged for the entirety of cellular tumor or infiltrating tumor (when present) regions in each patient sample relative to values in non-tumor tissues, colored low (gray) → high (red). Threshold was defined as 2 × the average rIOD in non-tumor samples. The eight possible combinations of three antigens are noted as I-VIII. Not all target antigens in each patient tumor sample showed expression above threshold. **C,** Euler diagram indicating the percentages of cellular tumor regions within the 43-patient cohort showing each of the eight possible expression patterns. The area of each ellipse is proportional to the percent of cellular tumor area expressing IL13Rα2, HER2 or EGFR, with overlap indicating co-expression within the tumor sample. **D**, Presumptive coverage of patients' cellular tumor regions assuming delivery of CAR T cells targeting one, two or three antigens.

illustrated in Figures 4E and 4F, where lines plot the ODs of IL13Rα2 and HER2, or IL13Rα2 and EGFR, immunoreactivities across a transect of pseudopalisading cells, changes in IL13Rα2 expression (red) could occur over 3-5 cell diameters, often but not always in parallel with HER2 immunoreactivity (green) (Figure 4E). In contrast, over the same transect, EGFR immunoreactivity (blue-white) was relatively uniform as compared to IL13Rα2 (red), decreasing only over areas devoid of cells (Figure 4F).

(c) Heterogeneity within subregions of cellular tumor

When multiple subregions of DAB immunostaining were identified by ImagePro within cellular tumor regions, antigen expression in these subregions could vary widely. This is illustrated by patient sample PBT025-1, in which all three target antigens were expressed in spatially disparate subregions. In this tumor sample, 11 subregions were identified, *a-k* in Figure 5A. Of these areas (Figure 5B; intensity coded light red → dark red), seven (*a, b, c, d, e, g,* and *i*) showed elevated levels of IL13Rα2, two (*f* and *j*) showed low IL13Rα2 levels, and two (*h* and *k*) were IL13Rα2 negative.

Overall, there were 13 tumor samples (of 43 total) within which multiple subregions of antigen expression were detected by the DAB plug-in to

ImagePro and could be considered individually (in the remainder, antigen expression in cellular regions was more spatially uniform). This variability was quantified by calculating the Shannon diversity index (*H*) for antigen expression each of these areas. Here, *H* is an index increasing in value with the numbers of antigens expressed and with greater differences in their relative abundance. In the majority of tumor samples (9 of 13), values of *H* were highly variable, indicating that levels of antigen expression across cellular tumor regions could be highly divergent. Only in tumor samples with the smallest number of subregions (PBT008, PBT018, PBT023, PBT029) were the values of *H* tightly clustered.

Inter-patient heterogeneity: variations of antigen expression between patients

We next assessed how tumor antigens were expressed in tumors considered as a whole across multiple patients. Our analysis is summarized in Figure 6B for regions of cellular tumor/pseudopalisading necrosis, and regions of infiltrating tumor when these were present (examples shown in Figure 6A). Observations were grouped according to the eight possible patterns of IL13Rα2, HER2, and EGFR expression, considered individually, and in combinations (designated I-VIII). Values of rIOD, presented as normalized

Table 1

Combinatorics of CAR T cell target antigen expression compared to predictions assuming random and independent expression of each antigen.

Group	POSSIBLE COMBINATIONS	Percent of eight combinations	PATIENT CELLULAR TUMOR REGIONS (n = 43)			PATIENT CELLULAR TUMOR SUBREGIONS (n = 109 from 13 patient samples)			TCGA (n = 543)		
			Observed counts	Observed percent	P observed vs. predicted	Observed counts	Observed percent	P observed vs. predicted	Observed counts	Observed percent	P observed vs. predicted
V	IL13Rα2 only	12.5%	2	4.7%	0.08	2	1.8%	<0.01	17	3.1%	<0.01
VII	HER2 only	12.5%	0	0.0%	<0.01	2	1.8%	<0.01	3	0.6%	<0.01
VI	EGFR only	12.5%	7	16.3%	0.29	34	31.2%	0.39	188	34.6%	<0.01
III	IL13Rα2 and HER2	12.5%	5	11.6%	0.55	8	7.3%	0.06	1	0.2%	<0.01
II	IL13Rα2 and EGFR	12.5%	5	11.6%	0.55	3	2.8%	<0.01	234	43.1%	<0.01
IV	HER2 and EGFR	12.5%	11	25.6%	0.01	17	15.6%	0.2	37	6.8%	<0.01
I	IL13Rα2 and HER2 and EGFR	12.5%	10	23.3%	0.04	30	27.5%	<0.01	41	7.6%	<0.01
VIII	Triple negative	12.5%	3	7.0%	0.2	14	12.8%	0.5	22	4.1%	<0.01

Difference between observed and expectation: above / none / below

Eight possible combinations of three antigens: IL13Rα2, HER2, EGFR. Data are by protein immunochemistry for patient samples and patient sample regions, and RNA expression profiling for TCGA. *P*-values are the result of the binomial test comparing the predicted and observed percentages with the null hypothesis that the samples are from the same distribution (one-tailed). **RED** = expression significantly above expectation; **BLUE** = expression significantly below expectation

to average values in non-tumor brain, are presented numerically and as color scale (gray → red). The immunostaining threshold for positive expression was defined as an rIOD twice the average in non-tumor brain.

While vagaries of antigen accessibility and antibody avidity confound quantitative comparisons between antigens, we take these measures of antigen expression relative to control tissue to be appropriate for semiquantitative comparisons of each antigen.

Within regions of cellular tumor, and infiltrating tumor when present, antigen expression varied markedly between patient samples, and, as expected, expression of multiple antigens was common. Within regions of infiltrating tumor, antigen expression patterns could be similar (50%; 8/16) or divergent (50%; 8/16) from those of cellular tumor regions. As infiltrating tumor was present in only a minority of our samples (37%; 16/43), we consider here only the cellular tumor regions present in all samples. For these regions of cellular tumor, the combinatorics of antigen expression are illustrated by the Euler diagram in Figure 6C. Except for EGFR, relatively few of the 43 tumor samples were scored as expressing single antigens (16.3% for EGFR, versus 4.7% for IL13Rα2 and none for HER2). Relatively more tumors were scored as double positive: 11.6% for EGFR and IL13Rα2; 11.6% for IL13Rα2 and HER2; 25.6% for EGFR and HER2). The percentage of triple positive tumors (IL13Rα2, HER2 and EGFR was 23.3%. Only 7.0% of samples were negative for all three antigens.

Overall, cellular tumor areas in 93.0% of patient samples expressed at least one of the three potential target antigens, and greater than 72.1% of tumors expressed two or three of these antigens. Based on these data, Figure 6D presents the percentages of patient tumors potentially targeted by single, dual, or triple CAR T cell therapies. Depending on the particular CAR T cell targets, multiple CAR T cell targeting increased potential patient coverage from as low as 51.2% for a single CAR to as high as 93.0% for all three CAR species.

Examination of mRNA expression in the TCGA database [47] yielded a similar pattern. Overall, when considered alone or in combination with other antigens, 54.0% (293/543) of tumors would be accessible to an IL13Rα2-CAR T cell, 15.1% (82/543) to a HER2-CAR T cell, and 92.1% (500/543) to an EGFR-CAR T cell.

*Non-random, non-independent expression of target antigens across patient tumor samples*

For regions of cellular tumor, we next assessed how the eight possible combinations of antigen immunoreactivity differed from patient to patient, using the compilation presented in Figure 6B. Here, our results were highly divergent from expectations assuming that the probability of expression of each antigen was random and equal, with no interdependency. As summarized in Table 1, across the entire 43-patient cohort, EGFR appeared with significantly higher than expected frequency when considered as a single antigen, when paired with HER2, and when in combination with IL13Rα2 and HER2. Of note, this dominance of EGFR expression was also evident within multiple subregions of cellular tumor regions (Figure 5, Table 1). This pattern was confirmed for the 543 patient tumors in the TCGA database [47], which also yielded patterns of antigen transcript expression that differed significantly from expectations of random and independent expression, with the largest divergence also seen for EGFR (Table 1).

We also examined the expression data in Figure 6B for potential associations of antigen expression (Figure 7A). Here, IL13Rα2 and HER2 expression showed preferential pairing, with expression of these antigens trending to be negatively associated with EGFR. A similar pattern was observed for TCGA mRNA expression data [47] (Figure 7B).

Discussion and conclusions

Summary of findings

Here, we have used immunohistochemistry to map cellular tumor regions of formalin-fixed paraffin-embedded (FFPE) tissues from patients with high-grade glioma (WHO grades III-IV) to evaluate spatially varying expression of clinically-relevant immunotherapy target antigens. We compared our
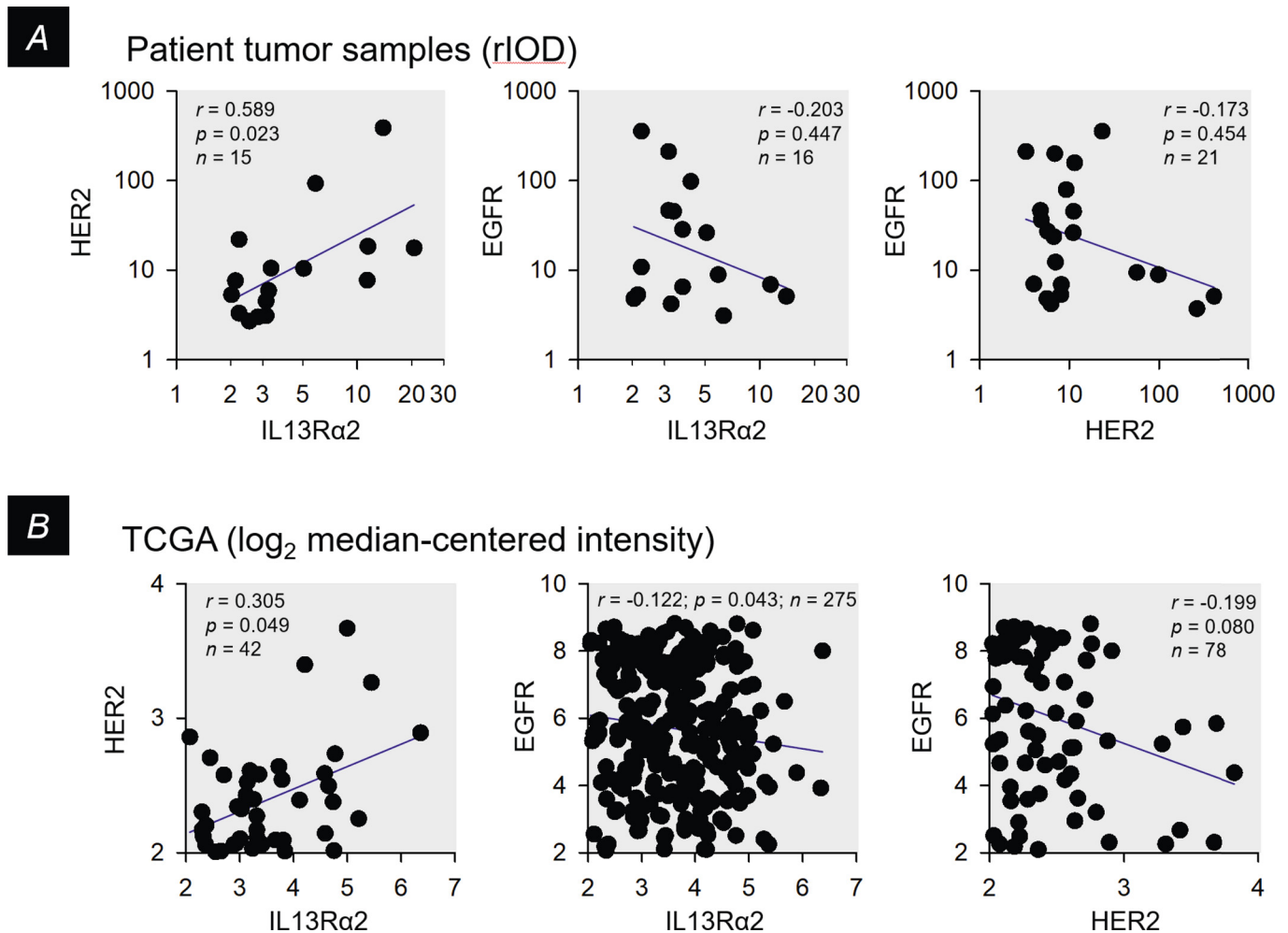
Figure 7. Examination of pair-wise correlations of IL13Rα2, HER2 and EGFR antigen expression within cellular regions of patient tumors. **A,** For patient tumor samples, correlation of IL13Rα2 and HER2 rIOD values, and anti-correlation of IL13Rα2 or HER2 with EGFR rIOD values, within cellular tumor regions for the subset of tumors showing above-threshold expression of both antigens (from Figure 6B). **B,** Similar presentation of mRNA expression profiles from the TCGA data set for glioblastoma [47], with threshold defined as 2-fold overexpression compared to control brain. In all graphs, blue lines are linear regressions to illustrate overall trends in the data.

measurements within the tumors of individual patients, and across multiple patients. To overcome the limitations of manual semi-quantitative scoring, as well as the subjectivity of visually evaluating of IHC staining, we employed digital imaging methods to more quantitatively examine expression of multiple antigens within tumor regions defined according to conventional neuropathology criteria.

We focused on three immunotherapy target antigens that are currently being utilized in clinical trials for recurrent high-grade glioma: IL13Rα2, HER2, and EGFR [7]. We observed that expression of these antigens was highly-variable, non-homogeneous, non-random, and non-independent. We observed this at all resolutions of our measurements: over the individual elements of 9.2 μm grids superimposed on cellular tumor areas, over 10 cm-scale regions of cellular tumor in tumor sections evaluated as a whole, and in subregions of pseudopalisading necrosis characteristic of glioblastoma.

Distributions of target antigen expression

Across entire cellular tumor regions in tumor sections, neighborhoods of EGFR expression could predominate over millimeter to centimeter-sized areas. In these tumors, neighborhoods of IL13Rα2 and HER2 expression

were quite compact, an example being PBT060 (Figure 2A1). In other tumors where EGFR expression was more spatially restricted, IL13Rα2 expression was progressively more expansive, as in PBT081 (Figure 2A2) and PBT068 (Figure 2A3). Finally, in tumors in which EGFR expression was minimal, such as PBT018, intermixed neighborhoods of IL13Rα2 and HER2 expression were seen (Figure 2B). When all of the tumor maps were arrayed in descending order of total percent of EGFR coverage (Supplemental Figure 1), a reciprocal relationship between spatial dominance of EGFR versus IL13Rα2/HER2 became apparent (Figure 3). This reciprocal pattern of EGFR and IL13Rα2/HER2 expression was preserved when tumor sections were evaluated as a whole (Figure 6B) and when plotted pair-wise (Figure 7A). TCGA mRNA expression profiles [47] showed a similar pattern (Figure 7B), suggesting that this relationship was not limited to our patient cohort.

Nonuniform spatially varying expression patterns have been seen for other cell-cell signaling elements in brain tumors: growth factors and their receptors including PDGF and PDGFR [48]; c-Met [49]; wild type EGFR and the EGFRvIII variant [38,39,50-52]; pro-angiogenic angiopoietin-2 [53]; and integrins αvβ3 and αvβ5 [54]. While the origins of these neighborhoods are not well understood, they impose a structure on tumor heterogeneity.

Interplay of hierarchical lineage and microenvironment shape glioma phenotypic variation

Overall, high-grade glioma may be viewed as highly complex microenvironment overlaid on developing tumor lineages to give rise to heterogeneous neighborhood organizations not unique to these target antigens [55–58].

Observations from single cell expression and genomic profiling [52,59-62] suggest that variegated glioma cell phenotypes derive in part from the cell-intrinsic variation found in diverging lineages [63,64] differentiating within a stem cell hierarchy [65], and recapitulating that of normal brain development [66], including appearance of cancer stem-like cells resembling normal stem cells [67]. That heterogeneity of target antigen expression is maintained down to the finest granularity available to us is consistent with a role of EGFR (and other receptor tyrosine kinases) amplification in shaping of individual glioma cell phenotypes.

Microenvironment also appears to be critical. Hypoxic niches are proposed to be dynamically regulated organizers of glioblastoma [68], including pseudopalisading necrosis [41]. Thus, the aligned tumor cells and their highly spatially restricted pattern of IL13Rα2 expression in neighborhoods of pseudopalisading necrosis may reflect a common association with hypoxia, as hypoxia is reported to up-regulate IL13Rα2 expression [69], and the distribution of IL13Rα2 was coincident with the layer of cells adjacent to the presumably hypoxic core [70]. A surrounding region of less severe hypoxia was characterized by HER2 expression and the cell migration assembling tumor palisades [41].

Other microenvironmental variations related to the physical position of neighborhoods within tumor masses also appear to contribute to establishing neighborhood phenotypes. Border niches, sites of progression and recurrence, can contain variegated populations of oligodendrocyte progenitor cells (OPCs), macrophages/microglia, and glioma stem cells [71]. Here, abnormal secretion of EGF by glioma-associated microglia is proposed to initiate a feedback loop promoting GBM invasion and functional disruption of brain tissue [72]. EGF secreting tumor cells counter this self-reinforcing process, as increased EGF is reported to result in loss of EGFR gene amplification [73].

Other aspects of metabolism may also be reflected in multiple local metabolic neighborhoods [74].

Between neighborhoods, systems of reciprocal interactions [75] may be operating [56,76-79]. The striking observation was that EGFR expression appeared anti-correlated with IL13Rα2 and HER2 at larger spatial scales, as suggested by both by our immunochemistry (Figure 7A) and by TCGA mRNA analyses (Figure 7B), may well indicate more widespread systems of mutual interactions.

Considerations for further development of glioma-directed immunotherapies

From a translational and clinical perspective, understanding patterns of tumor-related antigen expression in the context of high-grade glioma is an essential step towards developing effective immunotherapies.

One implication of our observations concerns the limited spatiotemporal sampling that can inform precision oncology for high-grade glioma [80]. Phenotypic and genetic aberrations [47,81,82] may be used to stratify patients and guide therapy choices [83]. We suggest the possibility, however, that the presence of highly variable phenotypic neighborhoods as reflected by regions of varying TCGA subtypes within individual tumors [63], by local and intermixed amplification of EGFR and other receptor tyrosine kinases [52], and by distortions of molecular heterogeneity in recurrent verses naïve tumors [84], may thwart application of narrowly targeted therapies [30]

Rather, as it is widely held that tumor recurrence has its origins in multiple preëxisting cell populations incorporating target antigen-deficient populations coming forward to fill the space (literally and in the evolutionary

sense) vacated by killed tumor cells [15-17,19,20,85], examinations of antigen escape have led to considerations of potentially more effective immunotherapies targeting multiple antigens simultaneously.

One recently explored strategy involves designing dual or triple targeting CAR T cell therapies to substantially increase the proportion of tumor cells in primary patient samples potentially targetable by immunotherapies, thereby reducing opportunities for antigen escape [42–44]. We suggest that the antigen expression patterns presented here indicate that multitarget immunotherapy targeting strategies incorporating EGFR along with IL13Rα2, HER2, or other targets, could be more clinically effective than antigen combinations omitting EGFR.

Alternatively, efforts are underway to design CARs recognizing immunotherapy targets broadly distributed within individual tumors and across patients. Examples include chondroitin sulfate proteoglycan 4 (CSPG4) [86] and the molecular complex bound by the scorpion-derived peptide chlorotoxin (CLTX) [87].

The evolutionary challenge of phenotypic heterogeneity in high-grade glioma

When considering the evolution of a species, theory posits that fitness in one environment does not necessarily guarantee fitness in a successor [88,89], and that genetic and phenotypic heterogeneity provides the raw material for adaptation under selection pressures [90,91]. This principle can be applied to consideration of malignancy, with the conclusion [92] that "… acquisition of phenotypic heterogeneity by populations of tumor cells imposes a degree of stability on the tumor as a whole". Thus, clinically, heterogeneity within tumors confers resilience to the challenges imposed by radiation, chemotherapies, electric fields, and immune-based therapies, resilience that ultimately leads to treatment failure and recurrence [14,93]. Or, from a patient's perspective, more extensive and dynamic heterogeneity of antigen expression correlates with less favorable prognoses [59,94]. Thus, evolutionary theory suggests that surmounting the consequences of the extensive heterogeneity of high-grade glioma will remain a major challenge to effective and durable therapies.

Financial Support

Declaration of Competing Interest

S.J.F. and C.E.B. receive royalty payments from Mustang Bio; S.J.F, C.E.B. and M.E.B. receive royalty payments from Chimeric Therapeutics; C.E.B. and M.E.B. have equity interests in Chimeric Therapeutics; all in areas outside of the work presented here. All other authors declare no competing interests.

CRediT authorship contribution statement

Michael E. Barish: Conceptualization, Methodology, Formal analysis, Data curation, Writing – original draft, Writing – review

References

[1] Stupp R, Mason WP, van den Bent MJ, Weller M, Fisher B, Taphoorn MJ, Belanger K, Brandes AA, Marosi C, Bogdahn U, Curschmann J, Janzer RC, Ludwin SK, Gorlia T, Allgeier A, Lacombe D, Cairncross JG, Eisenhauer E, Mirimanoff RO. European Organisation for Research and Treatment of Cancer Brain Tumor and Radiotherapy Groups, National Cancer Institute of Canada Clinical Trials Group, Radiotherapy plus concomitant and adjuvant temozolomide for glioblastoma. *N Engl J Med* 2005;**352**:987–96. doi:10.1056/NEJMoa043330.

[2] Stupp R, Taillibert S, Kanner A, Read W, Steinberg DM, Lhermitte B, Toms S, Idbaih A, Ahluwalia MS, Fink K, Di Meco F, Lieberman F, Zhu JJ, Stragliotto G, Tran DD, Brem S, Hottinger AF, Kirson ED, Lavy-Shahaf G, Weinberg U, Kim CY, Paek SH, Nicholas G, Burna J, Hirte H, Weller M, Palti Y, Hegi ME, Ram Z. Effect of tumor-treating fields plus maintenance temozolomide vs maintenance temozolomide alone on survival in patients with glioblastoma a randomized clinical trial. *JAMA - Journal of the American Medical Association* 2017;**318**:2306–16. doi:10.1001/jama.2017.18718.

3 Stupp R, Hegi ME. Targeting brain-tumor stem cells. *Nat Biotechnol* 2007;**25**:193–4. doi:10.1038/nbt0207-193.

4 Lim M, Xia Y, Bettegowda C, Weller M. Current state of immunotherapy for glioblastoma. *Nat Rev Clin Oncol* 2018;**15**:422–42. doi:10.1038/s41571-018-0003-5.

5 Irving M, de Silly RV, Scholten K, Dilek N, Coukos G. Engineering chimeric antigen receptor T-cells for racing in solid tumors: Don't forget the fuel. *Front Immunol* 2017;**8**:267. doi:10.3389/fimmu.2017.00267.

6 Mirzaei HR, Rodriguez A, Shepphird J, Brown CE, Badie B. Chimeric antigen receptors T cell therapy in solid tumor: Challenges and clinical applications. *Front Immunol* 2017;**8**:1850. doi:10.3389/fimmu.2017.01850.

7 Bagley SJ, Desai AS, Linette GP, June CH, O'Rourke DM. CAR T-cell therapy for glioblastoma: recent clinical advances and future challenges. *Neuro-oncol* 2018;**20**:1429–38. doi:10.1093/neuonc/noy032.

8 Watanabe K, Kuramitsu S, Posey AD, June CH. Expanding the therapeutic window for CAR T cell therapy in solid tumors: The knowns and unknowns of CAR T cell biology. *Front Immunol* 2018;**9**:2486. doi:10.3389/fimmu.2018.02486.

9 Akhavan D, Alizadeh D, Wang D, Weist MR, Shepphird JK, Brown CE. CAR T cells for brain tumors: Lessons learned and road ahead. *Immunol Rev* 2019;**290**:60–84. doi:10.1111/imr.12773.

10 Petersen CT, Krenciute G. Next generation CAR T cells for the immunotherapy of high-grade glioma. *Front Oncol* 2019;**9**:69. doi:10.3389/fonc.2019.00069.

11 Chuntova P, Downey KM, Hegde B, Almeida ND, Okada H. Genetically engineered T-cells for malignant glioma: Overcoming the barriers to effective immunotherapy. *Front Immunol* 2019;**9**:3062. doi:10.3389/fimmu.2018.03062.

12 Kwok D, Okada H. T-Cell based therapies for overcoming neuroanatomical and immunosuppressive challenges within the glioma microenvironment. *J Neurooncol* 2020;**147**:281–95. doi:10.1007/s11060-020-03450-7.

[13] Kurz SC, Wen PY. Quo Vadis—Do immunotherapies have a role in glioblastoma? *Current Treatment Options in Neurology* 2018;**20**. doi:10.1007/s11940-018-0499-0.

14 Qazi MA, Vora P, Venugopal C, Sidhu SS, Moffat J, Swanton C, Singh SK. Intratumoral heterogeneity: Pathways to treatment resistance and relapse in human glioblastoma. *Ann Oncol* 2017;**28**:1448–56. doi:10.1093/annonc/mdx169.

15 Sampson JH, Heimberger AB, Archer GE, Aldape KD, Friedman AH, Friedman HS, Gilbert MR, Herndon JE, McLendon RE, Mitchell DA, Reardon DA, Sawaya R, Schmittling RJ, Shi W, Vredenburgh JJ, Bigner DD. Immunologic escape after prolonged progression-free survival with epidermal growth factor receptor variant III peptide vaccination in patients with newly diagnosed glioblastoma. *J Clin Oncol* 2010;**28**:4722–9. doi:10.1200/JCO.2010.28.6963.

16 Brown CE, Badie B, Barish ME, Weng L, Ostberg JR, Chang WC, Naranjo A, Starr R, Wagner J, Wright C, Zhai Y, Bading JR, Ressler JA, Portnow J, D'Apuzzo M, Forman SJ, Jensen MC. Bioactivity and safety of IL13Ra2-redirected chimeric antigen receptor CD8+ T cells in patients with recurrent glioblastoma. *Clin Cancer Res* 2015;**21**:4062–72. doi:10.1158/1078-0432.CCR-15-0428.

17 Rapoport AP, Stadtmauer EA, Binder-Scholl GK, Goloubeva O, Vogl DT, Lacey SF, Badros AZ, Garfall A, Weiss B, Finklestein J, Kulikovskaya I, Sinha SK, Kronsberg S, Gupta M, Bond S, Melchiori L, Brewer JE, Bennett AD, Gerry AB, Pumphrey NJ, Williams D, Tayton-Martin HK, Ribeiro L, Holdich T, Yanovich S, Hardy N, Yared J, Kerr N, Philip S, Westphal S, Siegel DL, Levine BL, Jakobsen BK, Kalos M, June CH. NY-ESO-1-specific TCR-engineered T cells mediate sustained antigen-specific antitumor effects in myeloma. *Nat Med* 2015;**21**:914–21. doi:10.1038/nm.3910.

18 Brown CE, Alizadeh D, Starr R, Weng L, Wagner JR, Naranjo A, Ostberg JR, Blanchard MS, Kilpatrick J, Simpson J, Kurien A, Priceman SJ, Wang X, Harshbarger TL, D'Apuzzo M, Ressler JA, Jensen MC, Barish ME, Chen M, Portnow J, Forman SJ, Badie B, D'Apuzzo M, Ressler JA, Jensen MC, Barish ME, Chen M, Portnow J, Forman SJ, Badie B, D'Apuzzo M, Ressler JA, Jensen MC, Barish ME, Chen M, Portnow J, Forman SJ, Badie B. Regression of glioblastoma after chimeric antigen receptor T-cell therapy. *N Engl J Med* 2016;**375**:2561–9. doi:10.1056/NEJMoa1610497.

19 Krenciute G, Prinzing BL, Yi Z, Wu MF, Liu H, Dotti G, Balyasnikova IV, Gottschalk S. Transgenic expression of IL15 improves antiglioma activity of IL13Rα2-CAR T cells but results in antigen loss variants. *Cancer Immunol Res* 2017;**5**:571–81. doi:10.1158/2326-6066.CIR-16-0376.

20 O'Rourke DM, Nasrallah MP, Desai A, Melenhorst JJ, Mansfield K, Morrissette JJDD, Martinez-Lage M, Brem S, Maloney E, Shen A, Isaacs R, Mohan S, Plesa G, Lacey SF, Navenot J-MM, Zheng Z, Levine BL, Okada H, June CH, Brogdon JL, Maus MV, O'Rourke DM, Nasrallah MP, Desai A, Melenhorst JJ, Mansfield K, Morrissette JJDD, Martinez-Lage M, Brem S, Maloney E, Shen A, Isaacs R, Mohan S, Plesa G, Lacey SF, Navenot J-MM, Zheng Z, Levine BL, Okada H, June CH, Brogdon JL, Maus MV. A single dose of peripherally infused EGFRvIII-directed CAR T cells mediates antigen loss and induces adaptive resistance in patients with recurrent glioblastoma. *Sci Transl Med* 2017;**9**:eaaa0984. doi:10.1126/scitranslmed.aaa0984.

21 Bhate SS, Barlow GL, Schürch CM, Nolan GP. Tissue schematics map the specialization of immune tissue motifs and their appropriation by tumors. *Cell Syst* 2022;**13**:109–30. doi:10.1016/J.CELS.2021.09.012.

[22] Park JH, de Lomana ALG, Marzese DM, Juarez T, Feroze A, Hothi P, Cobbs C, Patel AP, Kesari S, Huang S, Baliga NS. A Systems Approach to Brain Tumor Treatment. *Cancers* 2021;**13**:3152. doi:10.3390/CANCERS13133152.

23 Debinski W, Gibo DM, Hulet SW, Connor JR, Gillespie GY. Receptor for interleukin 13 is a marker and therapeutic target for human high-grade gliomas. *Clin Cancer Res* 1999;**5**:985–90.

24 Ahmed N, Salsman VS, Kew Y, Shaffer D, Powell S, Zhang YJ, Grossman RG, Heslop HE, Gottschalk S. HER2-specific T cells target primary glioblastoma stem cells and induce regression of autologous experimental tumors. *Clin Cancer Res* 2010;**16**:474–85. doi:10.1158/1078-0432.CCR-09-1322.

25 Ahmed N, Brawley V, Hegde M, Bielamowicz K, Wakefield A, Ghazi A, Ashoori A, Diouf O, Gerken C, Landi D, Kalra M, Yi Z, Rooney C, Dotti G, Gee A, Heslop H, Gottschalk S, Powell S, Grossman R, Wels W, Kew Y, Baskin D, Zhang J, New P, Hicks J. Autologous HER2 CMV bispecific CAR T cells are safe and demonstrate clinical benefit for glioblastoma in a Phase I trial. *J Immunother Cancer* 2015;**3**:O11. doi:10.1186/2051-1426-3-S2-O11.

26 Ahmed N, Brawley V, Hegde M, Bielamowicz K, Kalra M, Landi D, Robertson C, Gray TL, Diouf O, Wakefield A, Ghazi A, Gerken C, Yi Z, Ashoori A, Wu MF, Liu H, Rooney C, Dotti G, Gee A, Su J, Kew Y, Baskin D, Zhang YJ, New P, Grilley B, Stojakovic M, Hicks J, Powell SZ, Brenner MK, Heslop HE, Grossman R, Wels WS, Gottschalk S. HER2-specific chimeric antigen receptor–modified virus-specific T cells for progressive glioblastoma: A phase 1 dose-escalation trial. *JAMA Oncol* 2017;**3**:1094–101. doi:10.1001/jamaoncol.2017.0184.

27 Chow KK, Naik S, Kakarla S, Brawley VS, Shaffer DR, Yi Z, Rainusso N, Wu M-F, Liu H, Kew Y, Grossman RG, Powell S, Lee D, Ahmed N, Gottschalk S. T cells redirected to EphA2 for the immunotherapy of glioblastoma. *Mol Ther* 2012;**21**:629–37. doi:10.1038/mt.2012.210.

28 Morgan RA, Johnson LA, Davis JL, Zheng Z, Woolard KD, Reap E, Feldman S, Chinnasamy N, Kuan C-T, Song H, Zhang W, Fine HA, Rosenberg SA. Recognition of glioma stem cells by genetically modified T cells targeting EGFRvIII and development of adoptive cell therapy for glioma. *Hum Gene Ther* 2012;**23**:1043–53. doi:10.1089/hum.2012.041.

29 Han J, Chu J, Keung Chan W, Zhang J, Wang Y, Cohen JB, Victor A, Meisen WH, Kim SH, Grandi P, Wang QE, He X, Nakano I, Chiocca EA, Glorioso JC, Kaur B, Caligiuri MA, Yu J. CAR-engineered NK cells targeting wild-type EGFR and EGFRvIII enhance killing of glioblastoma and patient-derived glioblastoma stem cells. *Sci Rep* 2015;**5**:1–13. doi:10.1038/srep11483.

30 Johnson LA, Scholler J, Ohkuri T, Kosaka A, Patel PR, McGettigan SE, Nace AK, Dentchev T, Thekkat P, Loew A, Boesteanu AC, Cogdill AP, Chen T, Fraietta JA, Kloss CC, Posey AD, Engels B, Singh R, Ezell T, Idamakanti N, Ramones MH, Li N, Zhou L, Plesa G, Seykora JT, Okada H, June CH, Brogdon JL, Maus MV. Rational development and characterization of humanized anti–EGFR variant III chimeric antigen receptor T cells for glioblastoma. *Sci Transl Med* 2015;**7** 275ra22-275ra22. doi:10.1126/scitranslmed.aaa4963.

31 Jarboe JS, Johnson KR, Choi Y, Lonser RR, Park JK. Expression of interleukin-13 receptor α2 in glioblastoma multiforme: Implications for targeted therapies. *Cancer Res* 2007;**67**:7983–6. doi:10.1158/0008-5472.CAN-07-1493.

32 Joshi BH, Puri RA, Leland P, Varricchio F, Gupta G, Kocak M, Gilbertson RJ, Puri RK. Identification of interleukin-13 receptor α2 chain overexpression in situ in high-grade diffusely infiltrative pediatric brainstem glioma. *Neuro-oncol* 2008;**10**:265–74. doi:10.1215/15228517-2007-066.

33 Kawakami M, Kawakami K, Takahashi S, Abe M, Puri RK. Analysis of interleukin-13 receptor α2 expression in human pediatric brain tumors. *Cancer* 2004;**101**:1036–42. doi:10.1002/cncr.20470.

34 Brown CE, Warden CD, Starr R, Deng X, Badie B, Yuan YC, Forman SJ, Barish ME. Glioma IL13Rα2 is associated with mesenchymal signature gene expression and poor patient prognosis. *PLoS One* 2013;**8**:e77769. doi:10.1371/journal.pone.0077769.

35 Koka V, Potti A, Forseen SE, Pervez H, Fraiman GN, Koch M, Levitt R. Role of Her-2/neu overexpression and clinical determinants of early mortality in glioblastoma multiforme. *Am J Clin Oncol* 2003;**26**:332–5. doi:10.1097/01.coc.0000020922.66984.e7.

36 Potti A, Forseen SE, Koka VK, Pervez H, Koch M, Fraiman G, Mehdi SA, Levitt R. Determination of HER-2/neu overexpression and clinical predictors of survival in a cohort of 347 patients with primary malignant brain tumors. *Cancer Invest* 2004;**22**:537–44. doi:10.1081/CNV-200026523.

37 Faulkner C, Palmer A, Williams H, Wragg C, Haynes HR, White P, DeSouza RM, Williams M, Hopkins K, Kurian KM. EGFR and EGFRvIII analysis in glioblastoma as therapeutic biomarkers. *Br J Neurosurg* 2015;**29**:23–9. doi:10.3109/02688697.2014.950631.

38 Biernat W, Huang H, Yokoo H, Kleihues P, Ohgaki H. Predominant expression of mutant EGFR (EGFRvIII) is rare in primary glioblastomas. *Brain Pathol* 2004;**14**:131–6. doi:10.1111/j.1750-3639.2004.tb00045.x.

39 Nishikawa R, Sugiyama T, Narita Y, Furnari F, Cavenee WK, Matsutani M. Immunohistochemical analysis of the mutant epidermal growth factor, ΔEGFR, in glioblastoma. *Brain Tumor Pathol* 2004;**21**:53–6. doi:10.1007/BF02484510.

40 Brennan CW, Verhaak RGW, McKenna A, Campos B, Noushmehr H, Salama SRR, Zheng S, Chakravarty D, Sanborn JZ, Berman SH, Beroukhim R, Bernard B, Wu C-JJ, Genovese G, Shmulevich I, Barnholtz-Sloan J, Zou L, Vegesna R, Shukla SA, Ciriello G, Yung WKKA, Zhang W, Sougnez C, Mikkelsen T, Aldape K, Bigner DD, Van Meir EG, Prados M, Sloan AE, Black KLL, Eschbacher J, Finocchiaro G, Friedman W, Andrews DW, Guha A, Iacocca M, O'Neill BP, Foltz G, Myers J, Weisenberger DJ, Penny R, Kucherlapati R, Perou CM, Hayes DN, Gibbs R, Marra M, Mills GB, Lander ES, Spellman P, Wilson RK, Sander C, Weinstein JN, Meyerson M, Gabriel SB, Laird PW, Haussler D, Getz G, Chin L, Van Meir EG, Prados M, Sloan AE, Black KL, Eschbacher J, Finocchiaro G, Friedman W, Andrews DW, Guha A, Iacocca M, O'Neill BP, Foltz G, Myers J, Weisenberger DJ, Penny R, Kucherlapati R, Perou CM, Hayes DN, Gibbs R, Marra M, Mills GB, Lander ES, Spellman P, Wilson RK, Sander C, Weinstein JN, Meyerson M, Gabriel SB, Laird PW, Haussler D, Getz G, Chin L, Benz C, Barrett W, Ostrom Q, Wolinsky Y, Bose B, Boulos PT, Boulos M, Brown J, Czerinski C, Eppley M, Kempista T, Kitko T, Koyfman Y, Rabeno B, Rastogi P, Sugarman M, Swanson P, Yalamanchii K, Otey IP, Liu YSY, Xiao Y, Auman JT, Chen PC, Hadjipanayis A, Lee E, Lee S, Park PJ, Seidman J, Yang LL, Kalkanis S, Poisson LM, Raghunathan A, Scarpace L, Bressler R, Eakin A, Iype L, Kreisberg RB, Leinonen K, Reynolds S, Rovira H, Thorsson V, Annala MJ, Paulauskis J, Curley E, Hatfield M, Mallery D, Morris S, Shelton T, Shelton C, Sherman M, Yena P, Cuppini L, DiMeco F, Eoli M, Maderna E, Pollo B, Saini M, Balu S, Hoadley KA, Li L, Miller CR, Shi Y, Topal MD, Wu J, Dunn G, Giannini C, Aksoy BA, Antipin Y, Borsu L, Cerami E, Gao J, Gross B, Jacobsen A, Ladanyi M, Lash A, Liang Y, Reva B, Schultz N, Shen R, Socci ND, Viale A, Ferguson ML, Chen QR, Demchok JA, Dillon LAL, Mills Shaw KR, Sheth M, Tarnuzzer R, Wang Z, Yang LL, Davidsen T, Guyer MS, Ozenberger BA, Sofia HJ, Bergsten J, Eckman J, Harr J, Smith C, Tucker K, Winemiller C, Zach LA, Ljubimova JY, Eley G, Ayala B, Jensen MA, Kahn A, Pihl TD, Pot DA, Wan Y, Hansen N, Hothi P, Lin B, Shah N, Yoon JG, Lau C, Berens M, Ardlie K, Carter SL, Cherniack AD, Noble M, Cho J, Cibulskis K, DiCara D, Frazer S, Gabriel SB, Gehlenborg N, Gentry J, Heiman D, Kim J, Jing R, Lawrence M, Lin P, Mallard W, Onofrio RC, Saksena G, Schumacher S, Stojanov P, Tabak B, Voet D, Zhang H, Dees NN, Ding L, Fulton LL, Fulton RS, Kanchi KL, Mardis ER, Wilson RK, Baylin SB, Harshyne L, Cohen ML, Devine K, Sloan AE, Van Den Berg SR, Berger MS, Carlin D, Craft B, Ellrott K, Goldman M, Goldstein T, Grifford M, Ma S, Ng S, Stuart J, Swatloski T, Waltman P, Zhu J, Foss R, Frentzen B, McTiernan R, Yachnis A, Mao Y, Akbani R, Bogler O, Fuller GN, Liu W, Liu YSY, Lu Y, Protopopov A, Ren X, Sun Y, Yung WKKA, Zhang J, Chen K, Weinstein JN, Bootwalla MS, Lai PH, Triche TJ, Van Den Berg DJ, Gutmann DH, Lehman NL, Brat D, Olson JJ, Mastrogianakis GM, Devi NS, Zhang Z, Lipp E, McLendon R. The somatic genomic landscape of glioblastoma. *Cell* 2013;**155**:462–77. doi:10.1016/j.cell.2013.09.034.

41 Brat DJ, Castellano-Sanchez AA, Hunter SB, Pecot M, Cohen C, Hammond EH, Devi SN, Kaur B, Van Meir EG. Pseudopalisades in glioblastoma are hypoxic, express extracellular matrix proteases, and are formed by an actively migrating cell population. *Cancer Res* 2004;**64**:920–7. doi:10.1158/0008-5472.CAN-03-2073.

[42] Hegde M, Corder A, Chow KKH, Mukherjee M, Ashoori A, Kew Y, Zhang YJ, Baskin DS, Merchant FA, Brawley VS, Byrd TT, Krebs S, Wu MF, Liu H, Heslop HE, Gottschalk S, Gottachalk S, Yvon E, Ahmed N. Combinational targeting offsets antigen escape and enhances effector functions of adoptively transferred T cells in glioblastoma. *Molecular Therapy* 2013;**21**:2087–101. doi:10.1038/mt.2013.185.

43 Hegde M, Mukherjee M, Grada Z, Pignata A, Landi D, Navai SA, Wakefield A, Fousek K, Bielamowicz K, Chow KKH, Brawley VS, Byrd TT, Krebs S, Gottschalk S, Wels WS, Baker ML, Dotti G, Mamonkin M, Brenner MK, Orange JS, Ahmed N. Tandem CAR T cells targeting HER2 and IL13Rα2 mitigate tumor antigen escape. *J Clin Invest* 2016;**126**:3036–52. doi:10.1172/JCI83416.

44 Bielamowicz K, Fousek K, Byrd TT, Samaha H, Mukherjee M, Aware N, Wu M-FF, Orange JS, Sumazin P, Man T-KK, Joseph SK, Hegde M, Ahmed N. Trivalent CAR T cells overcome interpatient antigenic variability in glioblastoma. *Neuro-oncol* 2018;**20**:506–18. doi:10.1093/neuonc/nox182.

45 Schindelin J, Arganda-Carreras I, Frise E, Kaynig V, Longair M, Pietzsch T, Preibisch S, Rueden C, Saalfeld S, Schmid B, Tinevez JY, White DJ, Hartenstein V, Eliceiri K, Tomancak P, Cardona A. Fiji: An open-source platform for biological-image analysis. *Nat Methods* 2012;**9**:676–82. doi:10.1038/nmeth.2019.

46 Micallef L, Rodgers P. eulerAPE: Drawing area-proportional 3-Venn diagrams using ellipses. *PLoS One* 2014;**9**:e101717. doi:10.1371/journal.pone.0101717.

47 McLendon R, Friedman A, Bigner D, Van Meir EG, Brat DJ, Mastrogianakis GM, Olson JJ, Mikkelsen T, Lehman N, Aldape K, Yung WKA, Bogler O, Weinstein JN, VandenBerg S, Berger M, Prados M, Muzny D, Morgan M, Scherer S, Sabo A, Nazareth L, Lewis L, Hall O, Zhu Y, Ren Y, Alvi O, Yao J, Hawes A, Jhangiani S, Fowler G, San Lucas A, Kovar C, Cree A, Dinh H, Santibanez J, Joshi V, Gonzalez-Garay ML, Miller CA, Milosavljevic A, Donehower L, Wheeler DA, Gibbs RA, Cibulskis K, Sougnez C, Fennell T, Mahan S, Wilkinson J, Ziaugra L, Onofrio R, Bloom T, Nicol R, Ardlie K, Baldwin J, Gabriel S, Lander ES, Ding L, Fulton RS, McLellan MD, Wallis J, Larson DE, Shi X, Abbott R, Fulton L, Chen K, Koboldt DC, Wendl MC, Meyer R, Tang Y, Lin L, Osborne JR, Dunford-Shore BH, Miner TL, Delehaunty K, Markovic C, Swift G, Courtney W, Pohl C, Abbott S, Hawkins A, Leong S, Haipek C, Schmidt H, Wiechert M, Vickery T, Scott S, Dooling DJ, Chinwalla A, Weinstock GM, Mardis ER, Wilson RK, Getz G, Winckler W, Verhaak RGW, Lawrence MS, O'Kelly M, Robinson J, Alexe G, Beroukhim R, Carter S, Chiang D, Gould J, Gupta S, Korn J, Mermel C, Mesirov J, Monti S, Nguyen H, Parkin M, Reich M, Stransky N, Weir BA, Garraway L, Golub T, Meyerson M, Chin L, Protopopov A, Zhang J, Perna I, Aronson S, Sathiamoorthy N, Ren G, Yao J, Wiedemeyer WR, Kim H, Sek WK, Xiao Y, Kohane IS, Seidman J, Park PJ, Kucherlapati R, Laird PW, Cope L, Herman JG, Weisenberger DJ, Pan F, Van Den Berg D, Van Neste L, Joo MY, Schuebel KE, Baylin SB, Absher DM, Li JZ, Southwick A, Brady S, Aggarwal A, Chung T, Sherlock G, Brooks JD, Myers RM, Spellman PT, Purdom E, Jakkula LR, Lapuk AV, Marr H, Dorton S, Yoon GC, Han J, Ray A, Wang V, Durinck S, Robinson M, Wang NJ, Vranizan K, Peng V, Van Name E, Fontenay GV, Ngai J, Conboy JG, Parvin B, Feiler HS, Speed TP, Gray JW, Brennan C, Socci ND, Olshen A, Taylor BS, Lash A, Schultz N, Reva B, Antipin Y, Stukalov A, Gross B, Cerami E, Wei QW, Qin LX, Seshan VE, Villafania L, Cavatore M, Borsu L, Viale A, Gerald W, Sander C, Ladanyi M, Perou CM, Hayes DN, Topal MD, Hoadley KA, Qi Y, Balu S, Shi Y, Wu J, Penny R, Bittner M, Shelton T, Lenkiewicz E, Morris S, Beasley D, Sanders S, Kahn A, Sfeir R, Chen J, Nassau D, Feng L, Hickey E, Barker A, Gerhard DS, Vockley J, Compton C, Vaught J, Fielding P, Ferguson ML, Schaefer C, Zhang J, Madhavan S, Buetow KH, Collins F, Good P, Guyer M, Ozenberger B, Peterson J, Thomson E. Comprehensive genomic characterization defines human glioblastoma genes and core pathways. *Nature* 2008;**455**:1061–8. doi:10.1038/nature07385.

48 Hermanson M, Funa K, Hartman M, Claesson-Welsh L, Heldin C-H, Westermark B, Nistér M. Platelet-derived growth factor and its receptors in human glioma tissue: Expression of messenger RNA and protein suggests the presence of autocrine and paracrine loops. *Cancer Res* 1992;**52**:3213–19.

49 Nabeshima K, Shimao Y, Sato S, Kataoka H, Moriyama T, Kawano H, Wakisaka S, Koono M. Expression of c-Met correlates with grade of malignancy in human astrocytic tumours: an immunohistochemical study. *Histopathology* 1997;**31**:436–43. doi:10.1046/j.1365-2559.1997.3010889.x.

50 Su Huang HJ, Nagane M, Klingbeil CK, Lin H, Nishikawa R, Ji XD, Huang CM, Gill GN, Wiley HS, Cavenee WK. The enhanced tumorigenic activity of a mutant epidermal growth factor receptor common in human cancers is mediated by threshold levels of constitutive tyrosine phosphorylation and unattenuated signaling. *J Biol Chem* 1997;**272**:2927–35. doi:10.1074/jbc.272.5.2927.

51 Inda MDM, Bonavia R, Mukasa A, Narita Y, Sah DWYY, Vandenberg S, Brennan C, Johns TG, Bachoo R, Hadwiger P, Tan P, DePinho RA, Cavenee W, Furnari F. Tumor heterogeneity is an active process maintained by a mutant EGFR-induced cytokine circuit in glioblastoma. *Genes Dev* 2010;**24**:1731–45. doi:10.1101/gad.1890510.

52 Snuderl M, Fazlollahi L, Le LP, Nitta M, Zhelyazkova BH, Davidson CJ, Akhavanfard S, Cahill DP, Aldape KD, Betensky RA, Louis DN, Iafrate AJ. Mosaic amplification of multiple receptor tyrosine kinase genes in glioblastoma. *Cancer Cell* 2011;**20**:810–17. doi:10.1016/j.ccr.2011.11.005.

[53] K. Koga, T. Todaka, M. Morioka, J.-I. Hamada, Y. Kai, S. Yano, A. Okamura, N. Takakura, T. Suda, Y. Ushio, Expression of Angiopoietin-2 in Human Glioma Cells and Its Role for Angiogenesis 1, 2001.

54 Bello L, Francolini M, Marthyn P, Zhang J, Carroll RS, Nikas DC, Strasser JF, Villani R, Cheresh DA, McL P. Black, $\alpha v \beta 3$ and $\alpha v \beta 5$ integrin expression in glioma periphery. *Neurosurgery* 2001;**49**:380–90. doi:10.1097/00006123-200108000-00022.

55 Yuan Y. Spatial heterogeneity in the tumor microenvironment. *Cold Spring Harb Perspect Med* 2016;**6**:a026583. doi:10.1101/cshperspect.a026583.

56 Broekman ML, Maas SLN, Abels ER, Mempel TR, Krichevsky AM, Breakefield XO. Multidimensional communication in the microenvirons of glioblastoma. *Nat Rev Neurol* 2018;**14**:1–14. doi:10.1038/s41582-018-0025-8.

57 Dirkse A, Golebiewska A, Buder T, Nazarov PV, Muller A, Poovathingal S, Brons NHC, Leite S, Sauvageot N, Sarkisjan D, Seyfrid M, Fritah S, Stieber D, Michelucci A, Hertel F, Herold-Mende C, Azuaje F, Skupin A, Bjerkvig R, Deutsch A, Voss-Böhme A, Niclou SP. Stem cell-associated heterogeneity in glioblastoma results from intrinsic tumor plasticity shaped by the microenvironment. *Nat Commun* 2019;**10**:1–16. doi:10.1038/s41467-019-09853-z.

[58] Chumakova AP, Hitomi M, Sulman EP, Lathia JD. High-throughput automated single-cell imaging analysis reveals dynamics of glioblastoma stem cell population during state transition. *Cytometry Part A* 2019;**95**:290–301. doi:10.1002/cyto.a.23728.

59 Patel AP, Tirosh I, Trombetta JJ, Shalek AK, Gillespie SM, Wakimoto H, Cahill DP, Nahed BV, Curry WT, Martuza RL, Louis DN, Rozenblatt-Rosen O, Suvà ML, Regev A, Bernstein BE. Single-cell RNA-seq highlights intratumoral heterogeneity in primary glioblastoma. *Science* 2014;**344**:1396–401. doi:10.1126/science.1254257.

60 Francis JM, Zhang CZ, Maire CL, Jung J, Manzo VE, Adalsteinsson VA, Homer H, Haidar S, Blumenstiel B, Pedamallu CS, Ligon AH, Love JC, Meyerson M, Ligon KL. EGFR variant heterogeneity in glioblastoma resolved through single-nucleus sequencing. *Cancer Discov* 2014;**4**:956–71. doi:10.1158/2159-8290.CD-13-0879.

61 Meyer M, Reimand J, Lan X, Head R, Zhu X, Kushida M, Bayani J, Pressey JC, Lionel AC, Clarke ID, Cusimano M, Squire JA, Scherer SW, Bernstein M, Woodin MA, Bader GD, Dirks PB. Single cell-derived clonal analysis of human glioblastoma links functional and genomic heterogeneity. *Proc Nat Acad Sci USA* 2015;**112**:851–6. doi:10.1073/pnas.1320611111.

62 Eskilsson E, Røsland GV, Solecki G, Wang Q, Harter PN, Graziani G, Verhaak RGW, Winkler F, Bjerkvig R, Miletic H. EGFR heterogeneity and implications for therapeutic intervention in glioblastoma. *Neuro-oncol* 2018;**20**:743–52. doi:10.1093/neuonc/nox191.

63 Sottoriva A, Spiteri I, Piccirillo SGMM, Touloumis A, Collins VP, Marioni JC, Curtis C, Watts C, Tavaré S, Tavare S, Tavaré S, Tavare S. Intratumor heterogeneity in human glioblastoma reflects cancer evolutionary dynamics. *Proc Nat Acad Sci USA* 2013;**110**:4009–14. doi:10.1073/pnas.1219747110.

64 Kim H, Zheng S, Amini SS, Virk SM, Mikkelsen T, Brat DJ, Grimsby J, Sougnez C, Muller F, Hu J, Sloan AE, Cohen ML, Van Meir EG, Scarpace L, Laird PW, Weinstein JN, Lander ES, Gabriel S, Getz G, Meyerson M, Chin L, Barnholtz-Sloan JS, Verhaak RGW. Whole-genome and multisector exome sequencing of primary and post-treatment glioblastoma reveals patterns of tumor evolution. *Genome Res* 2015;**25**:316–27. doi:10.1101/gr.180612.114.

65 Lan X, Jörg DJ, Cavalli FMG, Richards LM, Nguyen LV, Vanner RJ, Guilhamon P, Lee L, Kushida MM, Pellacani D, Park NI, Coutinho FJ, Whetstone H, Selvadurai HJ, Che C, Luu B, Carles A, Moksa M, Rastegar N, Head R, Dolma S, Prinos P, Cusimano MD, Das S, Bernstein M, Arrowsmith CH, Mungall AJ, Moore RA, Ma Y, Gallo M, Lupien M, Pugh TJ, Taylor MD, Hirst M, Eaves CJ, Simons BD, Dirks PB. Fate mapping of human glioblastoma reveals an invariant stem cell hierarchy. *Nature* 2017;**549**:227–32. doi:10.1038/nature23666.

66 Couturier CP, Ayyadhury S, Le PU, Nadaf J, Monlong J, Riva G, Allache R, Baig S, Yan X, Bourgey M, Lee C, Wang YCD, Wee Yong V, Guiot M-C, Najafabadi H, Misic B, Antel J, Bourque G, Ragoussis J, Petrecca K. Single-cell RNA-seq reveals that glioblastoma recapitulates a normal neurodevelopmental hierarchy. *Nat Commun* 2020;**11**:3406. doi:10.1038/s41467-020-17186-5.

[67] Bhaduri A, Di Lullo E, Jung D, Müller S, Crouch EE, Espinosa CS, Ozawa T, Alvarado B, Spatazza J, Cadwell CR, Wilkins G, Velmeshev D, Liu SJ, Malatesta M, Andrews MG, Mostajo-Radji MA, Huang EJ, Nowakowski TJ, Lim DA, Diaz A, Raleigh DR, Kriegstein AR. Outer radial glia-like cancer stem cells contribute to heterogeneity of glioblastoma. *Cell Stem Cell* 2020;**26**:48–63. doi:10.1016/j.stem.2019.11.015.

68 Evans SM, Judy KD, Dunphy I, Jenkins WTimothy, Hwang WT, Nelson PT, Lustig RA, Jenkins K, Magarelli DP, Hahn SM, Collins RA, Grady S, Koch CJ. Hypoxia is important in the biology and aggression of human glial brain tumors. *Clin Cancer Res* 2004;**10**:8177–84. doi:10.1158/1078-0432.CCR-04-1081.

[69] Minchenko OH, Tsymbal DO, Minchenko DO, Riabovol OO, Ratushna OO, Karbovskyi LL. Hypoxic regulation of the expression of cell proliferation related genes in U87 glioma cells upon inhibition of ire1 signaling enzyme. *Ukrainian Biochemical Journal* 2016;**88**:11–21. doi:10.15407/ubj88.01.011.

70 Sobhanifar S, Aquino-Parsons C, Stanbridge EJ, Olive P. Reduced expression of hypoxia-inducible factor-1α in perinecrotic regions of solid tumors. *Cancer Res* 2005;**65**:7259–66. doi:10.1158/0008-5472.CAN-04-4480.

[71] Hide T, Komohara Y, Miyasato Y, Nakamura H, Makino K, Takeya M, ichi Kuratsu J, Mukasa A, Yano S. Oligodendrocyte progenitor cells and macrophages/microglia produce glioma stem cell niches at the tumor border. *EBioMedicine* 2018;**30**:94–104. doi:10.1016/j.ebiom.2018.02.024.

72 Pudełek M, Król K, Catapano J, Wróbel T, Czyż J, Ryszawy D. Epidermal growth factor (EGF) augments the invasive potential of human glioblastoma multiforme cells via the activation of collaborative egfr/ros-dependent signaling. *Int J Mol Sci* 2020;**21**. doi:10.3390/ijms21103605.

73 William D, Mokri P, Lamp N, Linnebacher M, Classen CF, Erbersdobler A, Schneider B. Amplification of the EGFR gene can be maintained and modulated by variation of EGF concentrations in in vitro models of glioblastoma multiforme. *PLoS One* 2017;**12**:1–13. doi:10.1371/journal.pone.0185208.

74 Vartanian A, Singh SK, Agnihotri S, Jalali S, Burrell K, Aldape KD, Zadeh G. GBM's multifaceted landscape: Highlighting regional and microenvironmental heterogeneity. *Neuro-oncol* 2014;**16**:1167–75. doi:10.1093/neuonc/nou035.

75 Bonavia R, Inda MDM, Cavenee WK, Furnari FB. Heterogeneity maintenance in glioblastoma: A social network. *Cancer Res* 2011;**71**:4055–60. doi:10.1158/0008-5472.CAN-11-0153.

76 Jung E, Alfonso J, Osswald M, Monyer H, Wick W, Winkler F. Emerging intersections between neuroscience and glioma biology. *Nat Neurosci* 2019;**22**:1951–60. doi:10.1038/s41593-019-0540-y.

77 Pinto G, Brou C, Zurzolo C. Tunneling nanotubes: The fuel of tumor progression? *Trends Cancer* 2020;**6**:874–88. doi:10.1016/j.trecan.2020.04.012.

78 Montgomery MK, Kim SH, Dovas A, Zhao HT, Goldberg AR, Xu W, Yagielski AJ, Cambareri MK, Patel KB, Mela A, Humala N, Thibodeaux DN, Shaik MA, Ma Y, Grinband J, Chow DS, Schevon C, Canoll P, Hillman EMC. Glioma-induced alterations in neuronal activity and neurovascular coupling during disease progression. *Cell Rep* 2020;**31**:107500. doi:10.1016/j.celrep.2020.03.064.

[79] S. Jamous, A. Comba, P.R. Lowenstein, S. Motsch, Self-organization in brain tumors: How cell morphology and cell density influence glioma pattern formation, 16 (2020) e1007611. https://doi.org/10.1371/journal.pcbi.1007611.

80 Lee JK, Wang J, Sa JK, Ladewig E, Lee HO, Lee IH, Kang HJ, Rosenbloom DS, Camara PG, Liu Z, Van Nieuwenhuizen P, Jung SW, Choi SW, Kim J, Chen A, Kim KT, Shin S, Seo YJ, Oh JM, Shin YJ, Park CK, Kong DS, Seol HJ, Blumberg A, Il Lee J, Iavarone A, Park WY, Rabadan R, Nam DH. Spatiotemporal genomic architecture informs precision oncology in glioblastoma. *Nat Genet* 2017;**49**:594–9. doi:10.1038/ng.3806.

81 Phillips HS, Kharbanda S, Chen R, Forrest WF, Soriano RH, Wu TD, Misra A, Nigro JM, Colman H, Soroceanu L, Williams PM, Modrusan Z, Feuerstein BG, Aldape K. Molecular subclasses of high-grade glioma predict prognosis, delineate a pattern of disease progression, and resemble stages in neurogenesis. *Cancer Cell* 2006;**9**:157–73. doi:10.1016/j.ccr.2006.02.019.

82 Verhaak RG, Hoadley KA, Purdom E, Wang V, Qi Y, Wilkerson MD, Miller CR, Ding L, Golub T, Mesirov JP, Alexe G, Lawrence M, O'Kelly M, Tamayo P, Weir BA, Gabriel S, Winckler W, Gupta S, Jakkula L, Feiler HS, Hodgson JG, James CD, Sarkaria JN, Brennan C, Kahn A, Spellman PT, Wilson RK, Speed TP, Gray JW, Meyerson M, Getz G, Perou CM, Hayes DNN. Cancer Genome Atlas Research. Integrated genomic analysis identifies clinically relevant subtypes of glioblastoma characterized by abnormalities in PDGFRA, IDH1, EGFR, and NF1. *Cancer Cell* 2010;**17**:98–110. doi:10.1016/j.ccr.2009.12.020.

83 Eckel-Passow JE, Lachance DH, Molinaro AM, Walsh KM, Decker PA, Sicotte H, Pekmezci M, Rice T, Kosel ML, Smirnov IV, Sarkar G, Caron AA, Kollmeyer TM, Praska CE, Chada AR, Halder C, Hansen HM, McCoy LS, Bracci PM, Marshall R, Zheng S, Reis GF, Pico AR, O'Neill BP, Buckner JC, Giannini C, Huse JT, Perry A, Tihan T, Berger MS, Chang SM, Prados MD, Wiemels J, Wiencke JK, Wrensch MR, Jenkins RB. Glioma groups based on 1p/19q, IDH, and TERT promoter mutations in tumors. *N Engl J Med* 2015;**372**:2499–508. doi:10.1056/NEJMoa1407279.

84 Schäfer N, Gielen GH, Rauschenbach L, Kebir S, Till A, Reinartz R, Simon M, Niehusmann P, Kleinschnitz C, Herrlinger U, Pietsch T, Scheffler B, Glas M. Longitudinal heterogeneity in glioblastoma: Moving targets in recurrent versus primary tumors. *J Transl Med* 2019;**17**:96. doi:10.1186/s12967-019-1846-y.

85 Wang J, Cazzato E, Ladewig E, Frattini V, Rosenbloom DIS, Zairis S, Abate F, Liu Z, Elliott O, Shin YJ, Lee JK, Lee IH, Park WY, Eoli M, Blumberg AJ, Lasorella A, Nam DH, Finocchiaro G, Iavarone A, Rabadan R. Clonal evolution of glioblastoma under therapy. *Nat Genet* 2016;**48**:768–76. doi:10.1038/ng.3590.

86 Pellegatta S, Savoldo B, Di Ianni N, Corbetta C, Chen Y, Patané M, Sun C, Pollo B, Ferrone S, DiMeco F, Finocchiaro G, Dotti G. Constitutive and TNFα-inducible expression of chondroitin sulfate proteoglycan 4 in glioblastoma and neurospheres: Implications for CAR-T cell therapy. *Sci Transl Med* 2018;**10**. doi:10.1126/scitranslmed.aao2731.

87 Wang D, Starr R, Chang WC, Aguilar B, Alizadeh D, Wright SL, Yang X, Brito A, Sarkissian A, Ostberg JR, Li L, Shi Y, Gutova M, Aboody K, Badie B, Forman SJ, Barish ME, Brown CE. Chlorotoxin-directed CAR T cells for specific and effective targeting of glioblastoma. *Sci Transl Med* 2020;**12**:eaaw2672. doi:10.1126/scitranslmed.aaw2672.

[88] Gould SJ, Vrba ES. Exaptation—A missing term in the science of form. *Paleobiology* 1982;**8**:4–15.

[89] Gould SJ. *Wonderful Life: The Burgess Shale and the Nature of History*. W. W. Norton & Co.; 1989.

90 Gould SJ, Hildreth JEK, Booth AM. The evolution of alloimmunity and the genesis of adaptive immunity. *Q Rev Biol* 2004;**79**:359–82. doi:10.1086/426088.

91 Sánchez-Romero MA, Casadesús J. Contribution of phenotypic heterogeneity to adaptive antibiotic resistance. *Proc Nat Acad Sci USA* 2014;**111**:355–60. doi:10.1073/pnas.1316084111.

92 Fidler IJ. The Ernst W. Bertner Memorial Award lecture: the evolution of biological heterogeneity in metastatic neoplasms. *Symp Fundam Cancer Res* 1983;**36**:5–26.

93 Kleppe M, Levine RL. Tumor heterogeneity confounds and illuminates: Assessing the implications. *Nat Med* 2014;**20**:342–4. doi:10.1038/nm.3522.

94 Rajapakse VN, Herrada S, Lavi O. Phenotype stability under dynamic brain-tumor environment stimuli maps glioblastoma progression in patients. *Sci Adv* 2020;**6**:eaaz4125. doi:10.1126/sciadv.aaz4125.